PHYSICAL REVIEW D **93,** 115004 (2016)

Reconciling $(g-2)_\mu$ and charged lepton flavor violating processes through a doubly charged scalar

Joydeep Chakrabortty,[1] Pradipta Ghosh,[2] Subhadeep Mondal,[3] and Tripurari Srivastava[1]

[1]*Department of Physics, Indian Institute of Technology, Kanpur 208016, India*

[2]*Laboratoire de Physique Théorique, CNRS*[*]*, Univ. Paris-Sud, Université Paris-Saclay, 91405 Orsay, France and Centre de Physique Théorique, Ecole polytechnique, CNRS*[†]*, Université Paris-Saclay, 91128 Palaiseau, France*

[3]*Regional Centre for Accelerator-based Particle Physics, Harish-Chandra Research Institute, Jhunsi, Allahabad 211019, India*

(Received 10 February 2016; published 3 June 2016)

The scalar particle discovered at the Large Hadron Collider (LHC) has properties very similar to that of a standard model (SM) Higgs boson. Limited experimental knowledge of its model origin, as of now, however, does not rule out the possibility of accommodating this new particle into a beyond the SM (BSM) framework. A few of these schemes suggest that the observed scalar is just the *lightest* candidate of an enriched sector with several other heavier states *awaiting to be detected*. Such models with *nonminimal* scalar sector also accommodate other neutral and electrically charged (singly, doubly, triply, etc.) component fields as prescribed by the specific model. Depending on the mass and electric charge, these new states can produce potential signatures at colliders as well as in low-energy experiments. The presence of a doubly charged scalar, when accompanied by other neutral or charged scalar(s), can also generate neutrino masses. Adopting the second scenario, e.g., Babu-Zee construction, constraints from neutrino physics have been effaced in this study. Here, we investigate a few phenomenological consequences of a uncolored doubly charged scalar which couples to the charged leptons as well as gauge bosons. Restricting ourselves in the regime of conserved charged-parity (CP), we assume only a few nonzero Yukawa couplings ($y_{\mu\ell}$, where $\ell = e, \mu, \tau$) between the doubly charged scalar and the charged leptons. Our choices allow the doubly charged scalar to impinge low-energy processes like anomalous magnetic moment of muon and a few possible charged lepton flavor violating (CLFV) processes. These same Yukawa couplings are also instrumental in producing same-sign dilepton signatures at the LHC. In this article we examine the impact of individual contributions from the diagonal and off-diagonal Yukawa couplings in the light of muon $(g-2)$ excess. Subsequently, we use the derived information to inquire the possible CLFV processes and finally the collider signals from the decay of a doubly charged scalar. Our simplified analyses, depending on the mass of doubly charged scalar, provide a good estimate for the magnitude of the concerned Yukawa couplings. Our findings would appear resourceful to test the phenomenological significance of a doubly charged scalar by using complementary information from muon $(g-2)$, CLFV and the collider experiments.

DOI: 10.1103/PhysRevD.93.115004

I. INTRODUCTION

Discovery of a new scalar [1,2] has already proclaimed the success of LHC. This scalar has properties [3,4] quite identical to that of the SM Higgs boson, the only fundamental scalar within the SM framework. In the SM, the Higgs field emerges from an $SU(2)$ complex scalar doublet. A complete knowledge of the SM Higgs sector would require (i) measurements of the vacuum expectation value (VEV) acquired by the electrically neutral CP-even component of the aforementioned complex scalar doublet, (ii) the Higgs boson mass and (iii) the Higgs self coupling. At present, we have already probed the VEV of the SM through experimental measurements [5] and, have estimated the mass of a Higgs-like scalar boson at the LHC [3]. Thus, it remains to examine the only remaining parameter of the SM-Higgs sector, namely, the self-coupling. Unfortunately, the experimental sensitivity for the latter is very poor at the LHC and one perhaps needs to wait for the future colliders [6]. Hence, the possibility of having a Higgs-like scalar from BSM theories is certainly not redundant till date, especially when several other observations already ask for such an extension, e.g., non-zero neutrino masses and mixing [7–9]. Furthermore, mass of the newly discovered scalar [3] and the top-quark mass [5] strongly prefer the presence of one or more BSM scalars in the theory before 10^9–10^{11} GeV [10–13][1] (see also Refs. [15,16] for review). Introduction of these new scalars

[*]UMR 8627
[†]UMR 7644

[1]Some counter arguments also exist in this connection, as addressed in Ref. [14].

 © 2016 American Physical Society

assures stability of the SM-Higgs potential up to the Planck scale. Combining these observations, an extension of the SM Higgs sector seems rather plausible. For example, one can add extra scalar states which are encapsulated in different multiplets guided by the gauge symmetry and/or pattern of the symmetry breaking. A plethora of analyses [11,17–70] already exists in this connection where additional scalar mulitiplets are introduced to solve different shortcomings of the SM, like stability of the scalar potential up to the Planck scale, dark-matter, neutrino masses and mixing, etc.

These BSM scalar multiplets in general contain not only the electrically neutral fields but the charged (singly, doubly, triply, etc.) ones also. Phenomenology of these states may be constrained from the electroweak precision tests [5], e.g., see Refs. [55,71–73] for an extension with $SU(2)$ triplet Higgs. The presence of charged scalars, depending on the structure of the associated multiplet, at the same time can produce novel signals at the collider experiments, e.g., same-sign multileptons. Several analyses [42,52,72,74–109] are already performed in this direction, including experimental ones [110–126]. These charged scalars, apart from atypical LHC signatures, can also contribute to a class of low-energy phenomena that lead to lepton number as well as flavor violating processes. Such processes include CLFV (e.g. $\mu \to e\gamma$, μ to e conversion in atomic nuclei etc.) [58,62,76,94,107,127–141], neutrinoless double beta decay ($0\nu\beta\beta$) [42,53,58,62,88,107,134,142–147], rare meson decays (e.g., $M \to M'\ell_i\ell_j$, $M \to M'\ell_i\ell_j\ell_m\ell_n$) [148–151], muon $(g-2)$ [136,152] etc. Some of these processes, e.g., $0\nu\beta\beta$, rare-meson decays, etc. have one thing in common, i.e., they violate lepton number by 2 units which is the characteristic of a doubly-charged scalar.[2] The same doubly charged scalar can also participate in the CLFV processes and muon $(g-2)$. Several investigations, as aforesaid, do already exist concerning various phenomenological aspects of a doubly charged scalar. A dedicated entangled phenomenological inspection of the doubly-charged scalars, in the context of collider and low-energy experiments at the same time, however, still remains somewhat incomplete. This is exactly what we plan to do here and the current article is the first step toward a complete investigation. In passing we note that the other part of multiplets, i.e., the neutral scalar states can also show their own distinctive signals. For example, if these BSM neutral scalars are light, they can affect the SM-Higgs decay phenomenology through mixing. Phenomenological implications of additional neutral scalars are however, beyond the theme of this article and will not be addressed further.

We initiate our investigation with the discrepancy in anomalous magnetic moment of muon $\Delta a_\mu = a_\mu^{\rm exp} - a_\mu^{\rm th}$, which can be explained well in the presence of a doubly-charged scalar, $\Delta^{\pm\pm}$. Subsequently, we use this information to constrain *only the most relevant* associated Yukawa couplings that connect the doubly charged scalar with the charged leptons, i.e., $y_{\mu\ell}$ with $\ell = e, \mu, \tau$. In the next step, we investigate the allowed relevant CLFV processes in the presence of *the same set* of Yukawa couplings. At this level we scrutinize a new set of constraints on that *same set* of Yukawa couplings from the experimental limits on different CLFV processes. Finally, we explore the collider signals of a doubly charged scalar that appear feasible with the *chosen set* of Yukawa couplings and, are in agreement with the experimental constraints of $(g-2)_\mu$ and the relevant CLFV processes. However, like the existing literature we do not work in the context of any specific model. Rather, we parametrize the *unknown* model of doubly charged scalar in terms of a *few relevant* Yukawa couplings and the mass of the doubly charged scalar $(m_{\Delta^{\pm\pm}})$ that are resourceful to probe the existence of a doubly charged scalar experimentally. As a first attempt, we also stick to the regime of conserved CP. It is also important to emphasise that we focus on the range of[3] 400 GeV [126] $\lesssim m_{\Delta^{\pm\pm}} \lesssim$ 1000 GeV which is well accessible during run-II of the LHC.[4] Thus, in a nutshell, in this work we explore the possible correlations among $m_{\Delta^{\pm\pm}}$ and $y_{\mu\ell}$ as well as between different $y_{\mu\ell}$ in the context of (i) $(g-2)_\mu$ and (ii) a few CLFV processes. Thereafter, we use these information to study the possible $\Delta^{\pm\pm} \to \ell_\alpha^\pm \ell_\beta^\pm$ processes (i.e., same-sign dileptons) at the LHC.

It remains to mention one more important aspect associated with a $\Delta^{\pm\pm}$, i.e., the generation of nonzero neutrino masses and mixing. Accommodating massive neutrinos in the presence of a $\Delta^{\pm\pm}$ depends on the chosen theory framework which we will discuss later in Sec. II. Models of these kinds typically contain additional scalars (neutral, charged or both, depending on the concerned model) and a larger set of Yukawa couplings. This nonminimal set of Yukawa couplings (compared to $y_{\mu\ell}$) is essential to accommodate massive neutrinos simultaneously with an explanation for the $(g-2)_\mu$ anomaly, in the presence of a few CLFV processes. In the context of a minimal model (described later), we observed that the set of constraints on the relevant Yukawa couplings coming from the anomalous $(g-2)_\mu$ and nonobservation of the CLFV processes is rather independent to the ones required to satisfy the observed three flavor global neutrino data [7–9].

The paper is organized as follows, after the introduction we present a concise description of the underlying

[2]Presence of a Majorana fermion, for example right-handed neutrino, can also serve the same purpose, see Ref. [153] and references therein.

[3]The exclusion limit depends on the leptonic decay branching fractions of $\Delta^{\pm\pm}$ and one can safely take $m_{\Delta^{\pm\pm}} \geq 400$ GeV.

[4]One can always consider a large value for $m_{\Delta^{\pm\pm}}$ to suppress the CLFV processes. However, a heavier $\Delta^{\pm\pm}$ would result in a smaller production cross-section at the LHC and thereby ends in smaller number of signal events.

theoretical framework in Sec. II. Analytical expressions for the muon $(g-2)$ and a few possible CLFV processes are given in Secs. III and IV, respectively. We present results of our numerical analyses on Δa_μ and the allowed CLFV processes in Sec. V. Collider phenomenology of the $\Delta^{\pm\pm} \to \ell^\pm_\alpha \ell^\pm_\beta$ processes, following findings of the previous section is addressed in Sec. VI. Our conclusions are given in Sec. VII. Finally, a detail computation of the anomalous magnetic moment of muon through a doubly charged scalar is relegated in the appendix.

II. THE THEORY FRAMEWORK

The presence of a doubly charged scalar is possible in various representations, for example (i) an $SU(2)$ triplet[5] $\delta^T \equiv (\delta^{++}, \delta^+, \delta^0)$ with hypercharge, $Y = 1$ [21–25], (ii) an $SU(2)$ singlet κ^{++} with $Y = 2$ [33,53,155], (iii) left-right symmetric model [17–20], (iv) a quadruplet $\Sigma^T \equiv (\Sigma^{++}, \Sigma^+, \Sigma^0, \Sigma^-)$ with $Y = 1/2$ [137], (v) another doublet $\chi^T \equiv (\chi^{++}, \chi^+)$ with $Y = 3/2$ [52,74,89,156], (vi) a quintuplet $\Omega^T \equiv (\Omega^{++}, \Omega^+, \Omega^0, \Omega^-, \Omega^{--})$ with $Y = 0$ etc. The mulitiplets Σ and χ give rise to dimension-five while Ω produces dimension-six neutrino mass operators through their respective interactions with the SM fields. It is worth mentioning that a doubly charged scalar can also appear in a quintuplet with $Y > 0$ or in multiplets with larger isospins [50,98,137,157–159].

Phenomenological aspects of these multiplets are constrained from the electroweak precision observables [30,31,55,71–73,160–163], especially if the multiplet contains an electrically neutral component which develops a VEV. For the simplicity of analysis we however, focus solely on the doubly charged scalar without caring about the rest of multiplet members. This approach helps us to pin down the precise contributions from the doubly charged scalar. Furthermore, we assume negligible to vanishingly small VEV for the neutral scalar member of the associated multiplet, if any. The latter choice not only protects the ρ-parameter [5], but also guarantees the absence and(or) severe suppression of some of the couplings, e.g., $\Delta^{\pm\pm} W^\mp W^\mp$.

We are now ready to write down the relevant terms for our analysis. For the purpose of $(g-2)_\mu$ one needs to consider only terms like $y_{\mu\ell} \Delta^{\pm\pm} \mu^\mp \ell^\mp$. All other Yukawa couplings are taken to be zero and further, we assume $y_{\mu\ell} = y_{\ell\mu}$ as well as $y_{\mu e} = y_{\mu\tau}$. One must remain careful while interpreting these $y_{\mu\ell}$ where information about the specific model (see Refs. [99,101]) are also embedded. Our simplified choice of $y_{\mu\ell}$ leaves us with only three free parameters, namely $y_{\mu\mu}, y_{\mu e} (= y_{\mu\tau})$ and $m_{\Delta^{\pm\pm}}$ relevant for our analysis. It is apparent from our choice of Yukawa couplings that, along with $(g-2)_\mu$, a few CLFV processes like $\mu \to e\gamma$, $\tau \to \mu\gamma$, $\mu N \to e N^*$ (μ to e conversion in atomic nuclei) etc. are automatically switched on. We will elaborate this issue further in Sec. IV. Finally, we need to write down the relevant terms which lead to $pp \to \Delta^{\pm\pm}\Delta^{\mp\mp}$ process at the LHC. The necessary *trilinear* couplings between $\Delta^{\pm\pm}$ and the electroweak gauge-bosons, in the absence of VEV for the new multiplet, are given as [101]: $2ig_2 \sin\theta_W \Delta^{\pm\pm}\Delta^{\mp\mp} A_\sigma p^\sigma$ and $i(g_2/\cos\theta_W)(2 - Y - 2\sin^2\theta_W)\Delta^{\pm\pm}\Delta^{\mp\mp} Z_\sigma p^\sigma$, where p^σ is the momentum transfer at these vertices. Here, Y is hypercharge of the scalar multiplet that contains $\Delta^{\pm\pm}$, g_2 is the $SU(2)$ gauge coupling and θ_W is Weinberg angle [5]. It is important to note the structure of $\Delta^{\pm\pm}\Delta^{\mp\mp} Z_\mu$ vertex, where some knowledge of the underlying multiplet appears necessary through the hypercharge quantum number.[6]

A. Massive neutrinos with a $\Delta^{\pm\pm}$

In this subsection, as mentioned in the beginning, we aim to present a brief discussion about the neutrino mass generation in the presence of a $\Delta^{\pm\pm}$. Accommodating tiny neutrino masses in a model with $\Delta^{\pm\pm}$ can be achieved in different ways, e.g., in the tree-level from a Type-II seesaw mechanism using an $SU(2)$ triplet [21–25] or in the loop-level with an $SU(2)$ singlet doubly and another $SU(2)$ singlet singly (S^+) charged scalar [33] etc. However, a $\Delta^{\pm\pm}$ gets directly involved in the mechanism of neutrino mass generation only for the latter model and thus, we restrict our discussion only for this framework.

It turns out for the aforesaid scenario, better known as the Babu-Zee model [26,29,32,33], one needs a S^+ along with a $\Delta^{\pm\pm}$ to generate neutrino masses (m_ν) in the two-loop level. Now, let us assume that $y^s_{\ell\ell'}, y^d_{\ell\ell'}$ represent the *generic real* Yukawa couplings between the charged leptons and $S^+, \Delta^{\pm\pm}$, respectively with the following property: $y^{s(d)}_{\ell\ell'} = y^{s(d)}_{\ell'\ell}$. At this point if we set the scale of new physics (i.e., masses of $S^\pm, \Delta^{\pm\pm}$ and any other relevant parameter) $\sim\mathcal{O}(1\ \text{TeV})$, just for an example, then following Ref. [33] one can extract the following conditions:

(i) $\sum y^s_{\mu\ell} y^s_{\ell\mu} + \sum y^d_{\mu\ell} y^d_{\ell\mu} \sim \mathcal{O}(10)$ (from $(g-2)_\mu$ [164]),

(ii) $\sum y^s_{e\ell} y^s_{\ell\mu} + \sum y^d_{e\ell} y^d_{\ell\mu} \lesssim \mathcal{O}(0.001)$ (from $\mu \to e\gamma$ [165]) and

(iii) $y^d_{\mu\mu} y^{s^2}_{\mu\tau} (y^{s^2}_{e\tau} + y^{s^2}_{\mu\tau} + y^{s^2}_{e\mu})/(y^{s^2}_{e\tau} + y^{s^2}_{\mu\tau}) \sim 0.06$ and $(y^{s^2}_{e\tau} + y^{s^2}_{\mu\tau}) y^d_{\tau\tau} \sim 2 \times 10^{-4}$ (assuming $m_\nu \sim 0.1$ eV [166]).

At this point, let us assume that only $y^s_{\mu\mu}, y^d_{\mu\mu}$ are $\sim\mathcal{O}(1)$ while other associated y^s, y^d values remain at least $\lesssim 0.1$.

[5]It has been mentioned in Refs. [136,154], that in the context of neutrino mass generation using a scalar $SU(2)$ triplet, i.e., Type-II seesaw, it is normally difficult to generate additive contributions to muon $(g-2)$ from $(y^\dagger y)_{\mu\mu}$. One can nevertheless, generate an additive contribution to $(g-2)_\mu$ with $(y^2)_{\mu\mu}$ or $(y_{\mu\mu})^2$ [136].

[6]A complete knowledge of the underlying multiplet would also require information of the isospin.

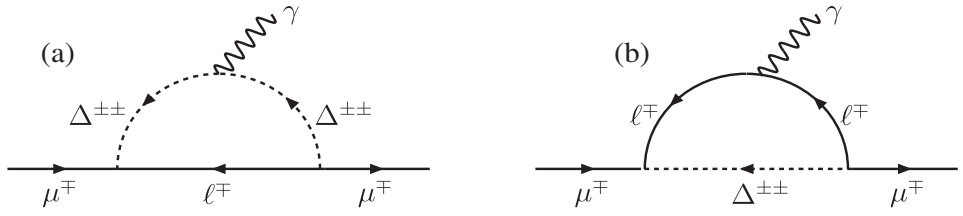

FIG. 1. Possible Feynman diagrams showing contributions to the muon anomalous magnetic moment through the exchange of a doubly charged scalar and the selected $y_{\mu\ell}$. The arrows represent the direction of electric charge flow.

Now one can easily satisfy condition (i) with $y^s_{\mu\mu} \sim 3$ and $y^d_{\mu\mu} \sim 1$. These chosen values can safely coexist with condition (ii) as long as (at least) $y^s_{e\mu}, y^d_{e\mu} \lesssim 0.001$ and $y^s_{e\tau}, y^d_{e\tau} \lesssim 0.01$. With these estimations one can rewrite condition (iii), up to a good approximation, as: $y^d_{\mu\mu} y^{s^2}_{\mu\tau} \sim 0.06$ and $y^{s^2}_{\mu\tau} y^d_{\tau\tau} \sim 2 \times 10^{-4}$. The former is trivially satisfied with $y^d_{\mu\mu} \sim 1$ and $y^s_{\mu\tau} \lesssim \mathcal{O}(0.1)$. The latter with $y^s_{\mu\tau} \lesssim \mathcal{O}(0.1)$ hints $y^d_{\tau\tau} \sim \mathcal{O}(0.01)$. Making the scale of new physics $\sim\mathcal{O}(500\ \text{GeV})$ one can get similar results, however, with reduced *upper bounds* on the concerned Yukawa couplings.

Collectively, playing with a larger set of Yukawa couplings, e.g., imposing hierarchical structures between y^d and y^s as well as among different flavor indices, one can always satisfy all the three aforementioned criteria. It is evident from conditions (i)–(iii), that the constraints from neutrino mass *simultaneously* put bounds on the off-diagonal y^s and diagonal y^d. On the contrary, limits from $(g-2)_\mu$ and CLFV processes constrain *independently* both the diagonal and off-diagonal y^s, y^d couplings. Thus, without emphasising the neutrino physics, one can safely work in a scenario when $y^s \to 0$. The remaining Yukawa couplings, namely y^ds, however, remain tightly constrained from the experimental limits on muon $(g-2)$ and CLFV processes. An analysis of the said kind, thus, provides maximum estimates for the associated y^d-type couplings. Any further attempt to add additional requirements for the same model, like neutrino mass generation, would only provide reduced upper bounds on the involved y^ds. Hence, for the rest of the work we keep on working with only y_d-type Yukawa couplings (henceforth read as $y_{\ell\ell'}$), imposing a minimal structure essential to account for the muon $(g-2)$ anomaly. We note in passing that, unless compensated by the relative mass hierarchies, the contribution to muon $(g-2)$ from a $\Delta^{\pm\pm}$ normally exceeds the same from a $S^{\pm}$ since $\Delta^{\pm\pm}\Delta^{\mp\mp}\gamma$, $S^{\pm}S^{\mp}\gamma$ vertices are sensitive to the electric charges of the concerned fields.

III. MUON $(g-2)$ WITH $\Delta^{\pm\pm}$

Precision measurements of the different low-energy processes always provide an acid test for the BSM theories. Observation of any possible disparity for these processes, compared to the corresponding SM predictions, provides a golden opportunity to explore as well as constrain various BSM models. The observed discrepancy in the anomalous magnetic moment of muon, Δa_μ is a very intriguing example of this kind.

In the SM, anomalous magnetic moment of muon is associated with the coupling $ig_2 \sin\theta_W\, \bar{\mu}\gamma^\sigma \mu A_\sigma$. However, even including the higher order contributions within the SM one can not explain the observed discrepancy $\Delta a_\mu = a^{\text{exp}}_\mu$ [167,168]-a^{th}_μ [169–172]. Here a^{exp}_μ is the experimentally measured value of $(g-2)_\mu$ and a^{th}_μ is the theoretical estimate of $(g-2)_\mu$ in the context of the SM. The latest numerical value[7] following Ref. [164] is given by

$$\Delta a_\mu = a^{\text{exp}}_\mu - a^{\text{th}}_\mu = (29.3 \pm 9.0) \times 10^{-10}. \qquad (1)$$

The presence of any possible BSM contribution will generally affect the $\mu \to \mu\gamma$ process at the loop level. In the presence of a $\Delta^{\pm\pm}$, the new BSM contributions to $(g-2)_\mu$ are shown in Fig. 1. From this figure one can see that a $\Delta^{\pm\pm}$ can contribute to $(g-2)_\mu$ through two possible ways. Following Refs. [174,175], new contribution[8] to $(g-2)_\mu$, in the presence of $\Delta^{\pm\pm}$ and allowing all the charged leptons in the loop, is given by:

$$\Delta a_\mu = \frac{f_m m_\mu^2 y^2_{\mu\ell}}{8\pi^2}\left[\int_0^1 d\rho \frac{2(\rho + \frac{m_\ell}{m_\mu})(\rho^2-\rho)}{[m_\mu^2\rho^2 + (m^2_{\Delta^{\pm\pm}} - m_\mu^2)\rho + (1-\rho)m_\ell^2]} - \int_0^1 d\rho \frac{(\rho^2 - \rho^3 + \frac{m_\ell}{m_\mu}\rho^2)}{[m_\mu^2\rho^2 + (m_\ell^2 - m_\mu^2)\rho + (1-\rho)m^2_{\Delta^{\pm\pm}}]}\right], \qquad (2)$$

where m_μ is the mass of muon [5] and m_ℓ is the mass of charged lepton "ℓ". We have also assumed real $y_{\mu\ell}$, so that $|y_{\mu\ell}|^2 = y^2_{\mu\ell}$. Further details of the computation are relegated to the appendix. In Eq. (2), f_m is equal to 1 for $\ell = e, \tau$ while equals to 4 for $\ell = \mu$. This multiplicative factor appears due to the presence of two identical fields in the interaction term.

[7]One should note that depending on the calculation of a^{th}_μ, the value of Δa_μ may change as pointed out in Ref. [173].

[8]We derive contributions from a $\Delta^{\pm\pm}$ (see appendix) in a way similar to the *Higgs type contribution* as shown in these references.

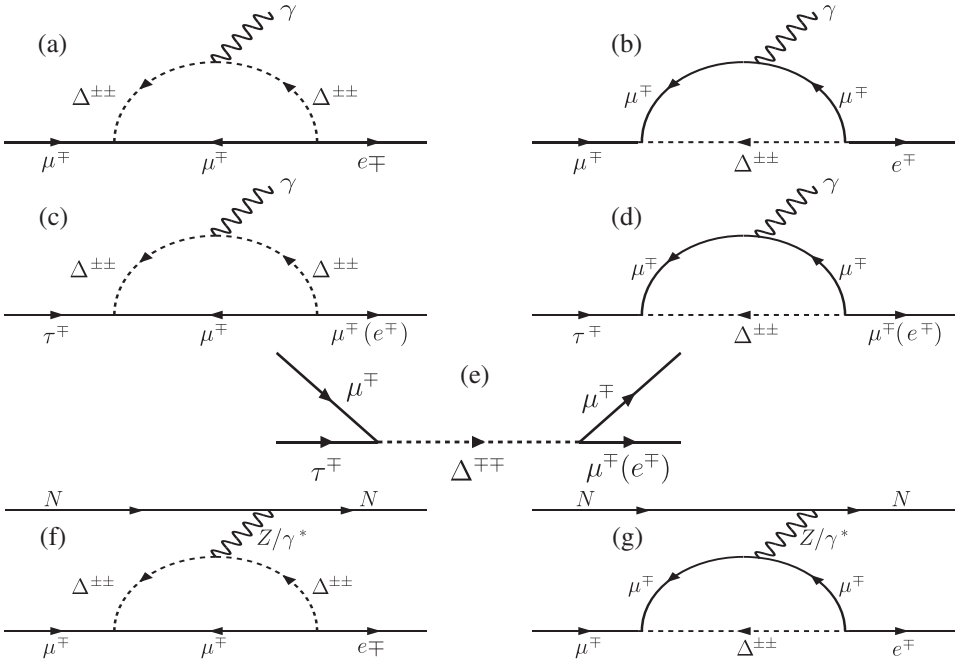

FIG. 2. Possible Feynman diagrams showing contributions to $\mu \to e\gamma(\mathrm{a,b}), \tau \to e\gamma, \tau \to \mu\gamma(\mathrm{c,d}), \tau \to 3\mu, \tau \to e\mu^+\mu^-(\mathrm{e})$ and $\mu N \to eN^*(\mathrm{f,g})$ processes in the presence of a $\Delta^{\pm\pm}$ and the selected $y_{\mu\ell}$s. Here, N represents the concerned atomic nucleus. The arrows represent the direction of electric charge flow.

IV. CLFV AND $\Delta^{\pm\pm}$

The most general Yukawa interactions between the charged leptons and a $\Delta^{\pm\pm}$ contains off-diagonal Yukawa couplings that are instrumental in producing CLFV processes like $\ell_i \to \ell_j\gamma$, $\ell_a \to \ell_b\ell_c\ell_d$ etc. In this article, however, we have assumed a minimal set of Yukawa couplings focusing on the muon anomalous magnetic moment. Thus, as already stated in Sec. II, our Yukawa sector contains only $y_{\mu\mu}$, $y_{\mu e}$ and $y_{\mu\tau}$, with $y_{\mu e} = y_{\mu\tau}$. Such a parameter choice would allow *only six* CLFV processes, namely $\mu \to e\gamma$, $\tau \to e\gamma$, $\tau \to \mu\gamma$, $\tau \to 3\mu$, $\tau \to e\mu^+\mu^-$ and $\mu N \to eN^*$ at the *respective leading orders*, that too with *only a few possible* diagrams. For the clarity of reading, we describe all such diagrams in Fig. 2. At this stage, it appears crucial to explain the phrase "only six CLFV processes at the leading orders" in order to ameliorate any possible delusion. It is absolutely true that the chosen set of $y_{\mu\ell}$ forbids tree-level processes like $\mu \to 3e, \tau \to \mu e^+e^-$ through an off-shell $\Delta^{\pm\pm}$, as sketched for $\tau \to e\mu^+\mu^-$ process in diagram (e) of Fig. 2.[9]

All the relevant branching fractions (Br) for the set of processes shown in Fig. 2 are given below [76,132,138,182]:

$$\mathrm{Br}(\mu \to e\gamma) = \frac{27\alpha_{\mathrm{em}}}{64\pi G_F^2 m^4_{\Delta^{\pm\pm}}} |(yy^\dagger)_{e\mu}|^2 \mathrm{Br}(\mu \to e\bar{\nu}_e\nu_\mu), \tag{3}$$

$$\mathrm{Br}(\tau \to e\gamma) = \frac{27\alpha_{\mathrm{em}}}{64\pi G_F^2 m^4_{\Delta^{\pm\pm}}} |(yy^\dagger)_{e\tau}|^2 \mathrm{Br}(\tau \to e\bar{\nu}_e\nu_\tau), \tag{4}$$

$$\mathrm{Br}(\tau \to \mu\gamma) = \frac{27\alpha_{\mathrm{em}}}{64\pi G_F^2 m^4_{\Delta^{\pm\pm}}} |(yy^\dagger)_{\mu\tau}|^2 \mathrm{Br}(\tau \to \mu\bar{\nu}_\mu\nu_\tau), \tag{5}$$

$$\mathrm{Br}(\tau \to 3\mu) = \frac{1}{4G_F^2 m^4_{\Delta^{\pm\pm}}} |y_{\tau\mu}|^2 |y_{\mu\mu}|^2 \mathrm{Br}(\tau \to \mu\bar{\nu}_\mu\nu_\tau), \quad \text{and} \tag{6}$$

$$\mathrm{Br}(\tau \to \mu\mu e) = \frac{1}{4G_F^2 m^4_{\Delta^{\pm\pm}}} |y_{\tau\mu}|^2 |y_{\mu e}|^2 \mathrm{Br}(\tau \to \mu\bar{\nu}_\mu\nu_\tau), \tag{7}$$

where $\alpha_{\mathrm{em}} = g_2^2 \sin^2\theta_W/4\pi$, G_F is the Fermi constant [5], $\mathrm{Br}(\mu \to e\bar{\nu}_e\nu_\mu) = 100\%$, $\mathrm{Br}(\tau \to e\bar{\nu}_e\nu_\tau) = 17.83\%$ and $\mathrm{Br}(\tau \to \mu\bar{\nu}_\mu\nu_\tau) = 17.41\%$ [5].

[9]These processes can show-up at the one-loop level via Z/γ^* mediator. Depending on the set of involved parameters process like $\ell_a \to \ell_i\ell_j\ell_k$ and also $\mu - e$ conversion in the nuclei may enjoy an extra enhancement from Z-penguin [176]. The latter can offer severe constraints on the parameter space compared to $\ell_i \to \ell_j\gamma$ processes [177–181], which normally holds true in the reverse order. However, following Ref. [181] one can conclude that such enhancement will not modify the scale of new physics ($m_{\Delta^{\pm\pm}}$ in our analysis) by orders of magnitudes. We, thus, do not consider these "enhancements" in our present analysis.

The rate of $\mu \to e$ conversion in atomic nuclei with the chosen set of $y_{\mu\ell}$ is written as

$$R(\mu N \to eN^*) = \frac{(\alpha_{\rm em} m_\mu)^5 Z_{\rm eff}^4 Z |F(q)|^2}{4\pi^4 m_{\Delta^{\pm\pm}}^4 \Gamma_{\rm capt}} \left| \frac{y^\dagger_{e\mu} y_{\mu\mu} F(r, s_\mu)}{3} - \frac{3(y^\dagger y)_{e\mu}}{8} \right|^2, \quad \text{where} \tag{8}$$

$$F(r, s_\mu) = \ln s_\mu + \frac{4s_\mu}{r} + \left(1 - \frac{2s_\mu}{r}\right)\sqrt{\left(1 + \frac{4s_\mu}{r}\right)} \times \ln \frac{\sqrt{(1 + \frac{4s_\mu}{r})} + 1}{\sqrt{(1 + \frac{4s_\mu}{r})} - 1},$$
$$r = -\frac{q^2}{m_{\Delta^{\pm\pm}}^2}, \qquad s_\mu = \frac{m_\mu^2}{m_{\Delta^{\pm\pm}}^2}. \tag{9}$$

Here, Z is the atomic number of the concerned nucleus. Values of $Z_{\rm eff}$, $\Gamma_{\rm capt}$ and $F(q^2 \backsimeq - m_\mu^2)$ for the different atomic nuclei can be obtained from Ref. [183].

Finally, before we start discussing our results in the next section, we summarize the present and the expected future limits of the considered CLFV processes in Table I.

TABLE I. The present and the expected future limits of the concerned CLFV processes.

CLFV processes	Present limit	Future limit
BR($\mu \to e\gamma$)	5.7×10^{-13} [165]	6.0×10^{-14} [184]
BR($\tau \to e\gamma$)	3.3×10^{-8} [185]	3.0×10^{-9} [186]
BR($\tau \to \mu\gamma$)	4.4×10^{-8} [185]	3.0×10^{-9} [186]
BR($\tau \to 3\mu$)	2.1×10^{-8} [187]	1.0×10^{-9} [186]
BR($\tau \to e\mu^+\mu^-$)	2.7×10^{-8} [187]	1.0×10^{-9} [186]
R($\mu N \to eN^*$) (for Au)	7.0×10^{-13} [188]	2.87×10^{-17} [189]

V. RESULTS

We initiate exploring our findings with the muon anomalous magnetic moment in the context of BSM input parameters $m_{\Delta^{\pm\pm}}$ and $y_{\mu\ell}(\equiv y_{\ell\mu})$. A self-developed FORTRAN code has been used for the purpose of numerical analyses. In our investigation we perform a scan over three free parameters $y_{\mu\mu}$, $y_{\mu e}(\equiv y_{\mu\tau})$ and $m_{\Delta^{\pm\pm}}$ in the following ranges: $10^{-4} \lesssim y_{\mu\mu}, y_{\mu e} \lesssim 1.2$ and 400 GeV$\lesssim m_{\Delta^{\pm\pm}} \lesssim$ 1000 GeV, respectively. For the analysis of $(g-2)_\mu$ we do not consider any constraints from the list of CLFV processes shown in Table I. In Fig. 3, we plot the variation of $y_{\mu\mu}$ with $m_{\Delta^{\pm\pm}}$ when (i) only $y_{\mu\mu}$ is contributing to Δa_μ (left plot), that is $\ell = \mu$ in Fig. 1 and, (ii) all the chosen $y_{\mu\ell}$s are contributing to Δa_μ (right plot). The left plot of Fig. 3 shows a copacetic correlation between $m_{\Delta^{\pm\pm}}$ and $y_{\mu\mu}$, as expected for an analysis with only two free parameters [see Eq. (2) with $y_{\mu\ell} = 0$ for $\ell \neq \mu$]. The smooth increase of $y_{\mu\mu}$ with larger $m_{\Delta^{\pm\pm}}$ values is also well understood from the same equation since $y_{\mu\mu}$ appears in the numerator while $m_{\Delta^{\pm\pm}}$ in the denominator. Hence, larger $y_{\mu\mu}$ values appear a must to satisfy the constraint on Δa_μ with increasing $m_{\Delta^{\pm\pm}}$. The blue and the green lines represent lower and upper bounds of the allowed one and two sigma (1σ–2σ) ranges for Δa_μ [see Eq. (1)], respectively. From the left plot one can also extract the possible range for $y_{\mu\mu}$, i.e., between 0.1–0.65 when $m_{\Delta^{\pm\pm}}$ varies within 400 GeV–1000 GeV. The astonishing correlation between $y_{\mu\mu}$ and $m_{\Delta^{\pm\pm}}$ gets distorted when one switches on the other off-diagonal Yukawa couplings, namely $y_{\mu e}$ and $y_{\mu\tau}$, as shown in the right plot of Fig. 3. These distortions are apparent only for the upper bands of allowed one and two sigma Δa_μ values while the lower bands remain practically the same as the scenario with only $y_{\mu\mu}$. Two conclusions become apparent from the right plot of Fig. 3: (1) off-diagonal Yukawa couplings can produce significant contributions to Δa_μ and, (2) these new contributions are normally negative and thus, one needs larger $y_{\mu\mu}$ values to accommodate the Δa_μ data. At the same time, the similarity of the lower one and two sigma lines, in both of the plots, implies that contributions from the off-diagonal $y_{\mu\ell}$s are typically smaller compared to the same from $y_{\mu\mu}$. Unlike the left plot, here one does not get a smooth increase in $y_{\mu\mu}$ value with increasing $m_{\Delta^{\pm\pm}}$. One can however, still estimate a range for $y_{\mu\mu}$, i.e., 0.1–1.2 for 400 GeV $\leq m_{\Delta^{\pm\pm}} \leq$ 1000 GeV.

In order to understand the relative contributions from $y_{\mu\mu}$ and $y_{\mu e}, y_{\mu\tau}$ to the computation of Δa_μ, we plot the four possible variations in Fig. 4. We consider the same range of $m_{\Delta^{\pm\pm}}$, i.e., 400 GeV $\lesssim m_{\Delta^{\pm\pm}} \lesssim$ 1000 GeV for these plots, similar to Fig. 3. All these data points (deep and light greens) satisfy the one and two sigma bounds on Δa_μ (represented by the light-brown and golden colored bands, respectively), as given in Eq. (1). Two plots in the top row of Fig. 4 show the variations of $\Delta a_\mu^{y_{\mu\mu}}$ with respect to $y_{\mu\mu}$ and the off-diagonal Yukawa couplings. Two of the bottom row plots represent the same but for $|\Delta a_\mu^{y_{\mu e} + y_{\mu\tau}}|$. Here, $\Delta a_\mu^{y_{\mu\mu}}$ is that part of Δa_μ which arises solely from $y_{\mu\mu}$ while $|\Delta a_\mu^{y_{\mu e} + y_{\mu\tau}}|$ represents the same from $y_{\mu\ell}$ with $\ell \neq \mu$ [see Eq. (2)]. From the top-left plot of Fig. 4, it is evident that in the presence of off-diagonal Yukawas, $y_{\mu\mu} \gtrsim 0.3$ can yield a large contribution to muon $(g-2)$ beyond 2σ. Thus, if we assume that contribution to Δa_μ arises solely from $y_{\mu\mu}$, i.e., $\Delta a_\mu \approx \Delta a_\mu^{y_{\mu\mu}}$, all points above the golden band remain experimentally excluded. The situation remains the same for $\Delta a_\mu^{y_{\mu\mu}}$ in the context of off-diagonal $y_{\mu\ell}$ when $y_{\mu e}$ or $y_{\mu\tau} \gtrsim 0.2$ (top-right plot for Fig. 4). Beyond $y_{\mu e} = 0.2$, the sizeable but opposite *sign* contributions ($-|\Delta a_\mu^{y_{\mu e} + y_{\mu\tau}}|$) from $y_{\mu\ell}$ adjust the positive over-growth of $\Delta a_\mu^{y_{\mu\mu}}$ beyond 2σ for $y_{\mu\mu} \gtrsim 0.3$, as shown in the bottom-right plot of Fig. 4. One more observation is apparent from the bottom-right plot of

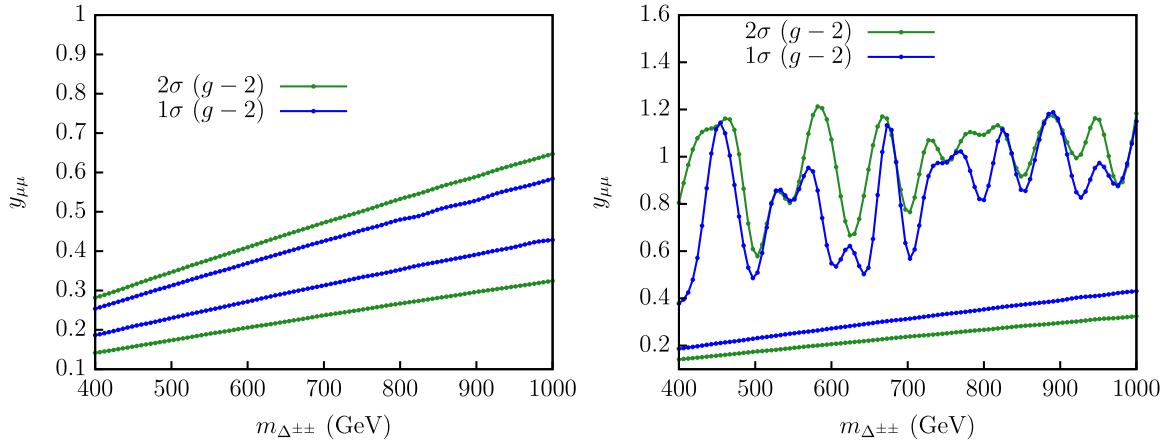

FIG. 3. Correlations between $m_{\Delta^{\pm\pm}}$ and $y_{\mu\mu}$ for the allowed one and two sigma ranges of Δa_μ. In the left plot Δa_μ is originating solely from $y_{\mu\mu}$ while in the right plot contributions from other off-diagonal $y_{\mu\ell}$s are also included. The blue and the green lines represent the one and two sigma bands of the allowed Δa_μ values, as given by Eq. (1).

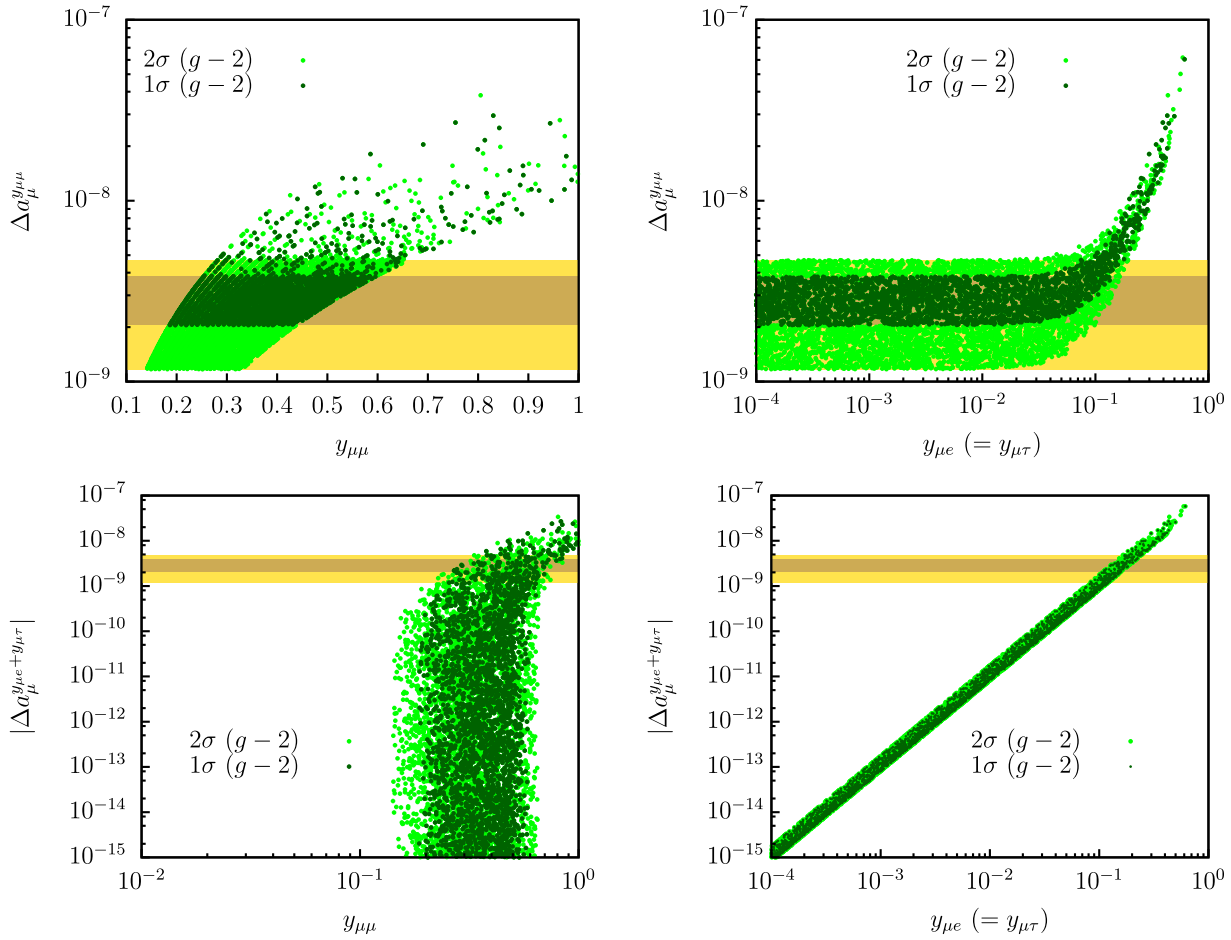

FIG. 4. Plots showing variations of $\Delta a_\mu^{y_{\mu\mu}}$ with $y_{\mu\mu}$ (top-left), $y_{\mu e}(\equiv y_{\mu\tau})$ (top-right) and the changes of $|\Delta a_\mu^{y_{\mu e}+y_{\mu\tau}}|$ with $y_{\mu\mu}$ (bottom-left), $y_{\mu e}(\equiv y_{\mu\tau})$ (bottom-right). The quantities $\Delta a_\mu^{y_{\mu\mu}}$ and $|\Delta a_\mu^{y_{\mu e}+y_{\mu\tau}}|$ are explained in the text. The light-brown and golden colored bands represent the measured 1σ and 2σ ranges of Δa_μ [see Eq. (1)]. The deep-green (light-green) colored point represents whether it satisfies the constraint on Δa_μ at the $1\sigma(2\sigma)$ interval. We consider 400 GeV $\lesssim m_{\Delta^{\pm\pm}} \lesssim$ 1000 GeV for these plots.

Fig. 4, that the contribution from $|\Delta a_\mu^{y_{\mu e}+y_{\mu\tau}}|$ in the determination of Δa_μ is practically negligible for $y_{\mu e} \lesssim 0.01$. On the contrary, as can be seen from the bottom-left plot of Fig. 4, that $|\Delta a_\mu^{y_{\mu e}+y_{\mu\tau}}|$ shows hardly any sensitivity to $y_{\mu\mu}$ below $y_{\mu\mu} \lesssim 0.3$. Only in the regime of $y_{\mu\mu} \gtrsim 0.3$, $|\Delta a_\mu^{y_{\mu e}+y_{\mu\tau}}|$ grows with $y_{\mu\mu}$. This growth becomes prominent for $y_{\mu\mu} \gtrsim 0.7$. So one can conclude that:

(1) For the region $y_{\mu\mu} \lesssim 0.3$, $y_{\mu e}(\equiv y_{\mu\tau}) \lesssim 0.01$, $\Delta a_\mu = \Delta a_\mu^{y_{\mu\mu}} + \Delta a_\mu^{y_{\mu e}+y_{\mu\tau}} \approx \Delta a_\mu^{y_{\mu\mu}}$. This is the reason why the lower one and two sigma lines for the two plots of Fig. 3 remain almost unaltered.

(2) In a tiny region: $0.3 \lesssim y_{\mu\mu} \lesssim 0.7$, $0.01 \lesssim y_{\mu e}(\equiv y_{\mu\tau}) \lesssim 0.2$, both of the contributions remain comparable to the measured Δa_μ [see Eq. (1)], i.e., $|\Delta a_\mu^{y_{\mu e}+y_{\mu\tau}}| \sim \Delta a_\mu^{y_{\mu\mu}} \sim \mathcal{O}(\Delta a_\mu)$. Hence, the measured constraint on Δa_μ appears feasible after a *tuned* cancellation between $\Delta a_\mu^{y_{\mu\mu}}$ and $\Delta a_\mu^{y_{\mu e}+y_{\mu\tau}}$.

(3) Finally, in the region with $y_{\mu\mu} \gtrsim 0.7$, $y_{\mu e}(\equiv y_{\mu\tau}) \gtrsim 0.2$, both of the contributions are larger than the measured Δa_μ (beyond the golden band at 2σ level). In other words, $|\Delta a_\mu^{y_{\mu e}+y_{\mu\tau}}| \sim \Delta a_\mu^{y_{\mu\mu}} \gg \mathcal{O}(\Delta a_\mu)$. Clearly, for this region, the parameter space that remains compatible with the measured constraint of Δa_μ appears through a *much-tuned* cancellation between $\Delta a_\mu^{y_{\mu\mu}}$ and $\Delta a_\mu^{y_{\mu e}+y_{\mu\tau}}$.

These last two features are also reflected in the erratic variation of $y_{\mu\mu}$, as shown in the right panel of Fig. 3.

A pictorial representation of these three aforesaid observations is shown in Fig. 5. Here, we plot the variations of individual components, i.e., $|\Delta a_\mu^{y_{\mu e}+y_{\mu\tau}}|$ and $\Delta a_\mu^{y_{\mu\mu}}$ with the total $\Delta a_\mu (\equiv \Delta a_\mu^{\rm tot})$. It is apparent from this plot that the contribution of $\Delta a_\mu^{y_{\mu\mu}}$ in the evaluation of $\Delta a_\mu^{\rm tot}$ is either the leading one (regime of overlap with the golden colored band at the 2σ interval) or overshooting. On the other hand, for a novel region of the parameter space $|\Delta a_\mu^{y_{\mu e}+y_{\mu\tau}}|$ remains subleading (left-hand side of the golden colored band) or comparable to $\Delta a_\mu^{y_{\mu\mu}}$ (regime of overlap with the golden band at the 2σ interval). Further, for $y_{\mu\ell}(\ell \neq \mu) \gtrsim 0.2$, $|\Delta a_\mu^{y_{\mu e}+y_{\mu\tau}}|$ can also overshoot $\Delta a_\mu^{\rm tot}$ like $\Delta a_\mu^{y_{\mu\mu}}$ (right-hand side of the golden band). However, this excess is opposite in sign to that of the $\Delta a_\mu^{y_{\mu\mu}}$ and thus, together they respect the 2σ constraint on $(g-2)_\mu$.

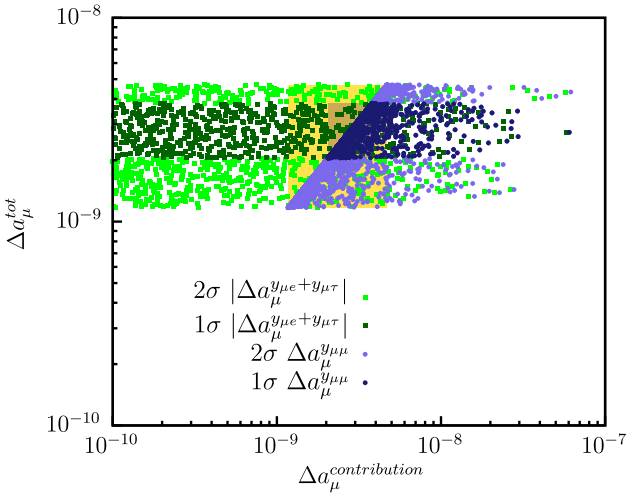

FIG. 5. Plot showing variations of the individual components, i.e., $|\Delta a_\mu^{y_{\mu e}+y_{\mu\tau}}|$ and $\Delta a_\mu^{y_{\mu\mu}}$ with the total $\Delta a_\mu (\equiv \Delta a_\mu^{\rm tot})$. The deep-green (light-green) colored point represents whether it satisfies the constraint of Δa_μ at the $1\sigma(2\sigma)$ interval for $|\Delta a_\mu^{y_{\mu e}+y_{\mu\tau}}|$. The deep-blue (light-blue) colored points represent the same for $\Delta a_\mu^{y_{\mu\mu}}$. Remaining details are the same as Fig. 4.

The discussion presented so far in the context of Δa_μ, using the information available from Figs. 3, 4, and 5, can be summarized as follows:

(1) For most of the parameter space, the dominant contribution to Δa_μ is coming from $y_{\mu\mu}$, irrespective of $y_{\mu\ell}(\ell \neq \mu)$ or $m_{\Delta^{\pm\pm}}$. This region is $y_{\mu e}(\equiv y_{\mu\tau}) \lesssim 0.01$, $0.1 \lesssim y_{\mu\mu} \lesssim 0.3$.

(2) The contribution of $y_{\mu\ell}$ in Δa_μ is always negative and practically negligible till $y_{\mu\ell} \sim 0.01$. In the range of $0.01 \lesssim y_{\mu\ell} \lesssim 0.2$, $y_{\mu\ell}$ can yield a contribution to $(g-2)_\mu$ comparable to that from $y_{\mu\mu}$ (i.e., when $0.3 \lesssim y_{\mu\mu} \lesssim 0.7$) but with an opposite sign. Lastly, beyond $y_{\mu\ell} \sim 0.2$, a large negative contribution from this parameter helps to nullify the positive overshooting contribution to Δa_μ from $y_{\mu\mu}$ with $y_{\mu\mu} > 0.7$.

(3) Depending on the chosen range of $m_{\Delta^{\pm\pm}}$, i.e., $400\ {\rm GeV} \lesssim m_{\Delta^{\pm\pm}} \lesssim 1000\ {\rm GeV}$, one can extract the upper bounds for the parameters $y_{\mu\mu}$ and $y_{\mu\ell}(\ell \neq \mu)$ from our analyses as 1.2 (see right-panel plot of Fig. 3) and 0.6 (see top-right plot of Fig. 4), respectively. These are the absolute possible upper limits of the respective parameters, as extracted through a simplified analysis. Adding other off-diagonal Yukawa couplings or introducing complex phases will in general result smaller upper bounds for the concerned parameters. The only trivial way to raise[10] these bounds is to consider a higher $m_{\Delta^{\pm\pm}}$. This in turn would yield a smaller production cross-section for the process $pp \to \Delta^{\pm\pm}\Delta^{\mp\mp}$ at the LHC and thereby enhancing the possibility of escaping the detection.

The investigation of muon $(g-2)$ has given us some useful information about the parameters $y_{\mu\mu}$, $y_{\mu\ell}(\ell \neq \mu)$ and $m_{\Delta^{\pm\pm}}$. We are now in a perfect platform to analyze the importance of these parameters in the context of suitable

[10]In the same spirit one can consider a lower $m_{\Delta^{\pm\pm}}$ to reduce the upper bounds on $y_{\mu\mu}, y_{\mu\ell}$. However, $m_{\Delta^{\pm\pm}}$ below 400 GeV is already at the edge of the experimentally excluded regions [126].

and relevant CLFV processes, as given in Table I. In order to perform this task, we do not consider the constraint from $(g-2)_\mu$. In this way, we can explore the *other allowed corner* of the parameter space for $y_{\mu\mu}$ and $y_{\mu\ell}$, focusing only on the CLFV processes. Subsequently, we will scrutinize mutual compatibility of the two allowed regions in $y_{\mu\mu}$ and $y_{\mu\ell}$ parameter space, as obtained from the $(g-2)_\mu$ and CLFV processes. However, to simplify our analysis we will use one key observation from our discussion of Δa_μ, i.e., in general $y_{\mu\mu} > y_{\mu\ell}$.

The expressions for the branching fractions or the rate of different CLFV processes are given in Eqs. (3)–(8). From these formulas it is evident that the allowed region in $y_{\mu\mu} - y_{\mu\ell}$ parameter space, consistent with the bounds shown in Table I, will expand with larger $m_{\Delta^{\pm\pm}}$ values. One can further extract another useful information from these expressions, i.e., $\mathrm{Br}(\tau \to e\gamma)$ and $\mathrm{Br}(\tau \to e\mu\mu)$ are the only two CLFV decays without any $y_{\mu\mu}$ contribution. Both of these processes are $\propto y_{\mu\ell}^2$ and thus, are in general suppressed compared to $\mathrm{Br}(\tau \to \mu\gamma)$ and $\mathrm{Br}(\tau \to 3\mu)$, respectively. At the same time, from the view point of present and the expected future limits (see Table I), $\mathrm{Br}(\tau \to e\gamma) \sim \mathcal{O}$ $(\mathrm{Br}(\tau \to \mu\gamma))$ and $\mathrm{Br}(\tau \to e\mu\mu) \sim \mathcal{O}$ $(\mathrm{Br}(\tau \to 3\mu))$. Hence, one can safely neglect the constraints coming from those two processes on the $y_{\mu\mu} - y_{\mu\ell}$ parameter space without any loss of generality. The latter statement has also been verified numerically. Thus, we do not consider constraints from these two channels in our numerical analysis as they will not affect our conclusions anyway.

We plot the allowed region of $y_{\mu\mu} - y_{\mu\ell}$ parameter space in Fig. 6 using the *individual* constraints on different CLFV processes as well as on Δa_μ, adopting one at a time. Further, we consider two extreme values of $m_{\Delta^{\pm\pm}}$, i.e., 400 GeV and 1000 GeV which cover the entire span. This choice would help us to understand the relative modification of the surviving $y_{\mu\mu} - y_{\mu\ell}$ parameter space for a change in $m_{\Delta^{\pm\pm}}$ value. It is clear from all the plots of Fig. 6 that

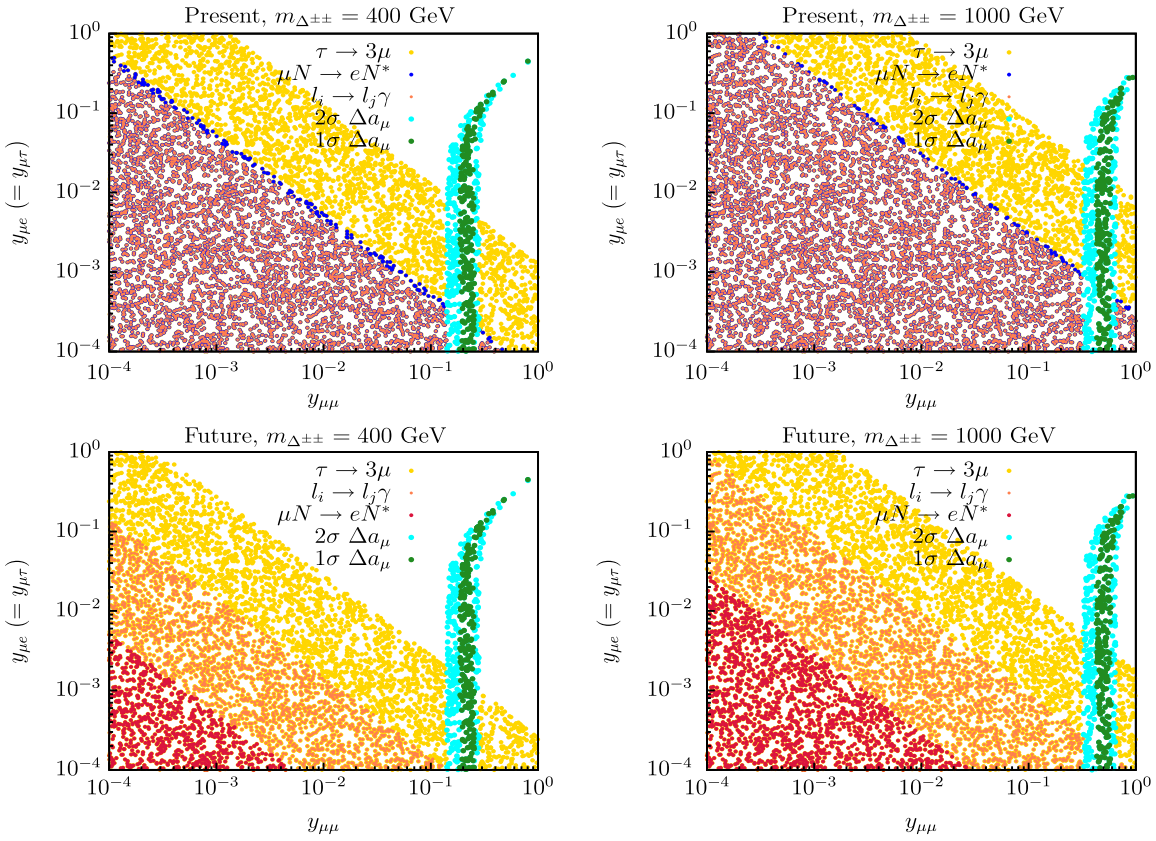

FIG. 6. Plots showing variations of $y_{\mu\mu}$ with $y_{\mu e}(\equiv y_{\mu\tau})$ in the context of CLFV processes: $\mu \to e\gamma$, $\tau \to \mu\gamma$ (collectively phrased as $\ell_i \to \ell_j\gamma$), $\tau \to 3\mu$, $\mu N \to eN^*$ and Δa_μ. The plots of the top row are drawn for $m_{\Delta^{\pm\pm}} = 400$ GeV (top-left) and $m_{\Delta^{\pm\pm}} = 1000$ GeV (top-right) assuming the existing constraints on various CLFV processes (see Table I). The sky-blue (deep-green) colored point represents whether it satisfies the constraint of Δa_μ at the $2\sigma(1\sigma)$ interval. The golden colored points (for all the four plots) are those which satisfy the constraint of only $\mathrm{Br}(\tau \to 3\mu)$. Deep-blue and dark-red colors (top-row) are used to represent those points which satisfy the constraint from only $\mu N \to eN^*$ process and only $\ell_i \to \ell_j\gamma$ process, respectively. The red and orange colored points are used to represent the same two quantities in the bottom row plots. The plots of the bottom row are drawn using the expected future limits on different allowed CLFV processes.

unlike $(g-2)_\mu$, the scales of $y_{\mu\mu}$ and $y_{\mu\ell}$ maintain some kind of reciprocal behavior. This phenomenon is expected since all the formulas of Eqs. (3)–(8) contain the product of Yukawa couplings in the form of $(y_{\mu\mu}y_{\mu\ell})$. The relative arenas of the allowed $y_{\mu\mu}-y_{\mu\ell}$ regions for the different CLFV processes are also well understood. It is apparent from Table I that at present the most stringent limit is coming from $\mu\to e\gamma$, followed by $\mu N\to eN^*$. On the other hand, the CLFV tau decays have much larger lower bounds, $\mathcal{O}(10^{-8})$. Hence, as expected, the allowed $y_{\mu\mu}-y_{\mu\ell}$ parameter space for $\mu\to e\gamma$ (thus for $\ell_i\to\ell_j\gamma$) lies in the bottom (dark-red points in the top-row plots of Fig. 6). This region is followed by the survived $y_{\mu\mu}-y_{\mu\ell}$ parameter space from $\mu N\to eN^*$ process, since the present limit on $R(\mu N\to eN^*)$ is marginally larger compared to the present bound on $\mathrm{Br}(\mu\to e\gamma)$. This feature is evident from the narrow visible strip of blue colored points as can be seen in both of the top-row plots of Fig. 6. Finally, rather *high* lower limit for $\tau\to 3\mu$ decay leaves a large allowed region in the $y_{\mu\mu}-y_{\mu\ell}$ space which is shown by the golden colored points. The strip in the $y_{\mu\mu}-y_{\mu\ell}$ parameter space which respects the constraint of Δa_μ is very narrow and given by the sky-blue (dark-green) colored points for the respective $2\sigma(1\sigma)$ limit [see Eq. (1)]. The presence of $m_{\Delta^{\pm\pm}}$ in the denominators [see Eqs. (3)–(8)] suggests an increase of the allowed $y_{\mu\mu}-y_{\mu\ell}$ parameter space with higher $m_{\Delta^{\pm\pm}}$ values. This behavior is visible from the two top-row plots of Fig. 6 where the surviving $y_{\mu\mu}-y_{\mu\ell}$ region grows larger for $m_{\Delta^{\pm\pm}}=1000$ GeV (top-right plot) compared to $m_{\Delta^{\pm\pm}}=400$ GeV scenario (top-left plot). Independent study of the allowed CLFV processes and $(g-2)_\mu$ suggests that only a very narrow region of the $y_{\mu\mu}-y_{\mu\ell}$ parameter space can survive the combined constraints from both. This region is about 0.15–0.3 for $y_{\mu\mu}$ while 0.0001–0.0004 for $y_{\mu\ell}$ when $m_{\Delta^{\pm\pm}}=400$ GeV (top-left plot of Fig. 6). The span for $y_{\mu\ell}$ increases slightly, i.e., 0.0001–0.0008 when one moves to $m_{\Delta^{\pm\pm}}=1000$ GeV (top-right plot of Fig. 6). The quantity $y_{\mu\mu}$, at the same time, just makes a small shift toward larger values, i.e., 0.3–0.6 without expanding the allowed region.

The two plots in the bottom row of Fig. 6 trail more or less a similar discussion, especially in the context of Δa_μ for which the allowed $y_{\mu\mu}-y_{\mu\ell}$ parameter space remains the same. This is not true for other processes since these plots are made using the expected future sensitivities of the allowed CLFV processes (see Table I). Now in the future, the quantity $R(\mu N\to eN^*)$ is expected to achieve a lower limit which is about four orders of magnitude smaller than the current bound. On the contrary, future sensitivities for $\mu\to e\gamma$ process and CLFV tau decays are only one order of magnitude smaller than the existing ones. Thus, in the future the most stringent constraint on the $y_{\mu\mu}-y_{\mu\ell}$ parameter space would come from $R(\mu N\to eN^*)$, as shown by the red colored points in the two bottom-row plots. The next most severe constraint will appear from $\mu\to e\gamma$ (hence for $\ell_i\to\ell_j\gamma$) which is represented by orange colored points. The golden colored points represent the surviving $y_{\mu\mu}-y_{\mu\ell}$ region from the constraint of $\tau\to 3\mu$ process. Once again, for each of these concerned processes, a larger allowed region in the $y_{\mu\mu}-y_{\mu\ell}$ parameter space appears as we move from $m_{\Delta^{\pm\pm}}=400$ GeV (bottom-left plot) to $m_{\Delta^{\pm\pm}}=1000$ GeV (bottom-right plot). The relative shrink of the allowed parameter space while using improved future bounds, compared to that with the present constraints, is natural. However, the important observation from the bottom-row plots of Fig. 6 is the complete disappearance of the region of overlap between the surviving $y_{\mu\mu}-y_{\mu\ell}$ parameter spaces from $R(\mu N\to eN^*)$ and $(g-2)_\mu$. The situation is practically the same for $\mathrm{Br}(\mu\to e\gamma)$ and $(g-2)_\mu$, although a tiny region of overlap would remain for $m_{\Delta^{\pm\pm}}=1000$ GeV (bottom-right plot). A sizeable region of overlap will still exist between $\mathrm{Br}(\tau\to 3\mu)$ and $(g-2)_\mu$ processes, however, smaller compared to the same with present constraints. So the region of $y_{\mu\mu}-y_{\mu\ell}$ parameter space that can survive the combined constraints from the possible CLFV processes and $(g-2)_\mu$ may disappear in the future. This missing area of overlap will certainly rule out the possibility of accommodating both the CLFV processes and $(g-2)_\mu$ in the context of a doubly charged scalar in the mass window of 400 GeV $\lesssim m_{\Delta^{\pm\pm}}\lesssim$ 1000 GeV. Nevertheless, one may observe a region of overlap like that of the top-row plots with larger values of $m_{\Delta^{\pm\pm}}$. The latter, as already stated, has rather less appealing collider phenomenology.

VI. $\Delta^{\pm\pm}$ AT THE LHC

In this final section of our analysis we investigate the collider phenomenology of a $\Delta^{\pm\pm}$ in the light of LHC run-II. Our knowledge about the parameters $y_{\mu\mu}, y_{\mu e}(\equiv y_{\mu\tau})$ and $m_{\Delta^{\pm\pm}}$, as we have acquainted in the last section thus, will appear resourceful. For the clarity of reading, it is important to reemphasize that so far we considered a few low-energy signatures *solely* from a $\Delta^{\pm\pm}$. Here, we study the pair-production of these $\Delta^{\pm\pm}$ having hypercharge $Y=1$ at the LHC and so, for our collider analysis. Thus, the coupling for $\Delta^{\pm\pm}\Delta^{\mp\mp}Z_\sigma$ vertex (see Sec. II) goes[11] as $i(g_2\cos 2\theta_W/\cos\theta_W)p^\sigma$. For other choices of the hypercharge one can simply scale this production cross-section, $\sigma(pp\xrightarrow{Z/\gamma}\Delta^{\pm\pm}\Delta^{\mp\mp})_{Y=1}$ as a function of g_2, Y and $\sin^2\theta_W$. Further, we also assume a negligible/vanishingly small VEV for the *possible* neutral scalar component of this $Y=1$ multiplet and hence, process like $\Delta^{\pm\pm}\to W^\pm W^\pm$ becomes irrelevant. In this scenario, the leading decay

[11]It is interesting to note that $\Delta^{\pm\pm}\Delta^{\mp\mp}Z_\sigma$ coupling reduces as ones goes from $Y=0$ to $Y=2$. For $Y>2$ or for a negative hypercharge, this coupling enhances.

modes for a $\Delta^{\pm\pm}$ are $\ell_\alpha^\pm \ell_\beta^\pm$ which are controlled by $y_{\mu\mu}$ and $y_{\mu e}/y_{\mu\tau}$. It is thus apparent that a set of *unconstrained* $y_{\mu\ell}(\ell = e, \mu, \tau)$ couplings will not only produce the same-sign same-flavor dileptons, e.g., $\Delta^{\pm\pm} \to \mu^\pm\mu^\pm$ but will also generate same-sign different-flavor dileptons, e.g., $\Delta^{\pm\pm} \to \mu^\pm e^\pm, \mu^\pm\tau^\pm$ with equal branching fractions. The last two decays are example of lepton flavor violating scalar decays.

At this point, our knowledge of $y_{\mu\mu}$, $y_{\mu e}(\equiv y_{\mu\tau})$ and $m_{\Delta^{\pm\pm}}$ from Sec. V appears very meaningful to estimate the relative strengths of different possible $\Delta^{\pm\pm} \to \ell_\alpha^\pm \ell_\beta^\pm$ processes. For our collider analysis, just like our two previous investigations of a few CLFV processes and $(g-2)_\mu$, we consider $400\ \text{GeV} \lesssim m_{\Delta^{\pm\pm}} \lesssim 1000\ \text{GeV}$, following the exclusion limit set by the LHC run-I data-set [126]. At the same time, from Sec. V, we can observe an allowed region in the $y_{\mu\mu} - y_{\mu\ell}(\ell \neq \mu)$ parameter space that survives *the combined set of present* constraints from muon $(g-2)$ and a few CLFV processes. In this region of survival, one gets $y_{\mu\ell} \sim \mathcal{O}(10^{-4})$ while $y_{\mu\mu} \sim \mathcal{O}(10^{-1})$ (see two top-row plots of Fig. 6). It is hence needless to mention that at the LHC processes like $\Delta^{\pm\pm} \to \mu^\pm e^\pm$ or $\Delta^{\pm\pm} \to \mu^\pm\tau^\pm$ will remain orders of magnitude suppressed compared to $\Delta^{\pm\pm} \to \mu^\pm\mu^\pm$ mode, provided one respects the combined constraints coming from $(g-2)_\mu$ and a few CLFV processes. Unfortunately, as discussed in Sec. V, such a conclusion would not hold true in the future when the $y_{\mu\mu} - y_{\mu\ell}(\ell \neq \mu)$ parameter space that can survive the combined constraints of $(g-2)_\mu$ and CLFV processes remains missing. One should note that such a region in the parameter space can reappear for large $m_{\Delta^{\pm\pm}}$ values, but at the cost of a diminished $\sigma(pp \xrightarrow{Z/\gamma} \Delta^{\pm\pm}\Delta^{\mp\mp})$. From the aforementioned discussion one can conclude that with our simplified parameter choice, the region of parameter space which respects the combined constraints of muon $(g-2)$ and some CLFV processes will predominantly yield four-muon $(pp \to \Delta^{\pm\pm}\Delta^{\mp\mp} \to 2\mu^\pm 2\mu^\mp)$ final state at the LHC.

For the sake of numerical analyses, the parton level signal events are generated using CalcHEP [190]. These events are then passed through PYTHIA v6.4.28 [191] for decay, showering, hadronization, and fragmentation. PYCELL has been used for the purpose of jet construction. We have used CTEQ6L parton distribution function [192] while generating the events. Factorization and renormalization scales are set at $\sqrt{\hat{s}}$ (i.e, $\mu_R = \mu_F = \sqrt{\hat{s}}$), where $\sqrt{\hat{s}}$ is the parton level center-of-mass energy. We work in the context of LHC with 13 TeV center-of-mass energy and used the following set of *basic* selection cuts to identify isolated leptons[12] $(l = e, \mu)$ and jets (hadronic) in the final states:

(i) A final state lepton must have $p_T^l > 10$ GeV and $|\eta^l| < 2.5$.
(ii) A final state jet is selected if $p_T^j > 20$ GeV and $|\eta^j| < 2.5$.
(iii) Lepton-lepton separation,[13] $\Delta R_{ll} > 0.2$.
(iv) Lepton-photon separation, $\Delta R_{l\gamma} > 0.2$.
(v) Lepton-jet separation, $\Delta R_{lj} > 0.4$.
(vi) Hadronic energy deposition, $\sum p_T^{\text{had}}$ around an isolated lepton must be $< 0.2 \times p_T^l$.
(vii) Final states with four-leptons are selected if the leading and subleading leptons have $p_T^l > 30$ GeV while for the remaining two, $p_T^l > 20$ GeV.

Leading SM background contribution will arise from $t\bar{t}Z/\gamma^*$ or ZZ/γ^* events. However, one can use the two following characteristics to suppress these backgrounds: (1) Four-lepton final states from $t\bar{t}Z/\gamma^*$ channels always appear with certain amount of missing transverse energy ($\not{E}_T$). (2) The set of four-leptons coming from ZZ process contains pairwise same flavor opposite-sign leptons from a Z-decay, and can easily be eliminated using appropriate invariant mass (m^{inv}) cuts which is isomorphic to *Z-veto*. Background events are generated using MadGraph5@aMCNLO v2.2.3 [193,194] and subsequently showered with PYTHIA. In our background simulations, we switched on all the possible processes that lead to $pp \to 2\mu^\mp 2\mu^\pm$ final state with at most two jets (light or b-tagged). At this stage, after a careful scrutiny of the different kinematic distributions for both the signal (S) and background (B) events, we have introduced the following set of *advanced* cuts to guarantee an optimized signal to background event ratio:

C1: Within the chosen framework a $\Delta^{\pm\pm}$ decays only into $\mu^\pm\ell^\pm(\ell = e, \mu, \tau)$ and hence, one would expect no hadronic jets for the final states. However, hadronic jets may appear while showering and we therefore, limit the final state hadronic jet multiplicity up to one.

C2: We further impose another criterion on the possible final state hadronic-jet, i.e., it must not be a b-tagged jet. This choice helps to reduce the $t\bar{t}Z/\gamma^*$ background.

C3: Theoretically, no source of $\not{E}_T$ exists for the predominant decay mode $\Delta^{\pm\pm} \to \mu^\pm\mu^\pm$ although nonzero $\not{E}_T$ can appear from subleading $\Delta^{\pm\pm} \to \mu^\pm\tau^\pm$ mode. The latter, as discussed in Sec. V, remains highly suppressed. Hence, we consider an upper limit of 30 GeV on the $\not{E}_T$.

C4: In our analysis, a pair of same-sign leptons emerges from a $\Delta^{\pm\pm}$ whereas for the backgrounds, a pair of opposite-sign leptons shares the same source. We therefore, construct m^{inv} for all the possible final state opposite-sign lepton pairs and discard all those events with $|m^{\text{inv}}_{l^+l^-} - m_Z| \leq 15$ GeV. Here, m_Z is the mass of Z-boson.

[12]Final states with τ-jets (from a hadronically decaying tau) are discarded.

[13]ΔR is defined as $\sqrt{(\Delta\Phi)^2 + (\Delta\eta)^2}$, where $\Delta\Phi$ is the difference in involved azimuthal angles while $\Delta\eta$ is the difference of concerned pseudorapidities, respectively.

TABLE II. Signal cross-sections for the three chosen benchmark points before and after applying the selection-cuts as described in the text. The final row represents the total cross-section from all the possible SM backgrounds which contain four-muon final states with a maximum hadronic-jet multiplicity of two.

	Parameters			
Benchmark points	$m_{\Delta^{\pm\pm}}$ (GeV)	$y_{\mu\mu}$	Production cross-section (fb)	Cross-section after cuts (fb)
BP1	600	0.29	1.52	0.286
BP2	800	0.46	0.33	0.061
BP3	1000	0.47	0.08	0.014
SM backgrounds	All inclusive		11.56	0.01

This cut appears useful to suppress backgrounds from Z-boson decay.

In Table II, we show the signal cross-sections prior and after implementing all the basic and advanced cuts. In this context, following the discussion of last section, we consider a set of three representative benchmark points which simultaneously satisfies the present set of bounds on CLFV processes and $(g-2)$ of muon. The same discussion also predicts $y_{\mu\mu} \gg y_{\mu\ell}(\ell \neq \mu)$ with $y_{\mu\mu} \sim \mathcal{O}(0.1)$ and $y_{\mu\ell} \sim \mathcal{O}(10^{-4})$. Thus, we do not explicitly mention the corresponding values of $y_{\mu e}(\equiv y_{\mu\tau})$ in Table II. In the context of numbers presented in Table II, it is interesting to explore the effectiveness of the *advanced* cuts, e.g., C3, C4. We have observed that the advanced selection cut C3 reduces 22% of the background events while diminishes 18% of the signal events (BP1 for example). Subsequent application of cut C4 kills 4% of the surviving events for the signal (BP1) whereas removes 99% of the surviving background events.

Finally, in Fig. 7 we show the variation of statistical significance[14] as a function of the integrated luminosity $(\mathcal{L})$, for a set of three possible benchmark points (see Table II). The integrated luminosity range (starting from 1 fb^{-1} up to the proposed maximum) for the LHC and the high-luminosity LHC (HL-LHC) [195]) are represented with golden and dark-golden color, respectively. The horizontal black colored line represents a 3σ statistical significance. The diminishing nature of statistical significance with increasing $m_{\Delta^{\pm\pm}}$ (see benchmark points in Table II) is a natural consequence of reducing $\sigma(pp \to \Delta^{\pm\pm}\Delta^{\mp\mp})$. One can compensate this reduction with a higher center-of-mass energy or larger $\mathcal{L}$, as can be seen from Fig. 7. It is evident from this figure that one would expect strong experimental evidence (statistical significance $\geq 4\sigma$) of a $\Delta^{\pm\pm}$ (as sketched within our construction) up to $m_{\Delta^{\pm\pm}} \approx 800$ GeV during the ongoing LHC run-II. The exact time line is however, $m_{\Delta^{\pm\pm}}$ dependent. For example, a discovery (statistical significance $\geq 5\sigma$) of the studied $\Delta^{\pm\pm}$ up to $m_{\Delta^{\pm\pm}} \approx 600$ GeV appears possible with $\mathcal{L} = 100$ fb^{-1}, which is well envisaged by 2017–2018. A similar conclusion for $m_{\Delta^{\pm\pm}} = 800$ GeV at the 4σ level however, needs $\mathcal{L} = 300$ fb^{-1} and hence, could appear feasible around 2020. For a more massive $\Delta^{\pm\pm}$ discovery, e.g., $m_{\Delta^{\pm\pm}} = 1000$ GeV, one would undoubtedly require a larger $\mathcal{L}$ like 3000 fb^{-1}. Necessity of such a high $\mathcal{L}$ would leave a massive $\Delta^{\pm\pm}$ undetected at the LHC. The proposed high-luminosity extension of the LHC, HL-LHC [195], however, will certainly explore this scenario. We note in passing that a $\Delta^{\pm\pm}$ much heavier than 1000 GeV would remain hidden even in such a powerful machine. The latter, however, will leave its imprints through a region in the $y_{\mu\mu} - y_{\mu\ell}(\ell \neq \mu)$ parameter space (see Fig. 6) that would simultaneously respect the improved future bounds on a few CLFV processes and muon $(g-2)$.

[14]Calculated as $S/\sqrt{S+B}$ where $S(B)$ represents the number of signal(background) events.

VII. SUMMARY AND CONCLUSIONS

Discovery of a "Higgs-like" scalar at the LHC and hitherto incomplete knowledge about its origin have revived the quest for an extended scalar sector beyond the SM. An interesting possibility is to consider these

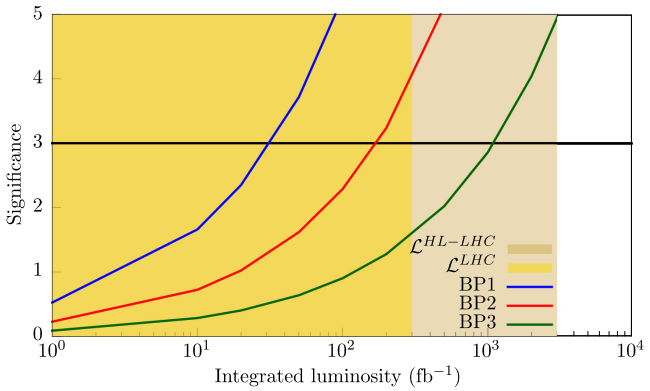

FIG. 7. Variation of the statistical significance as a function of the integrated luminosity $(\mathcal{L})$ for the three different benchmark points (see Table II). The black colored horizontal line represents a 3σ statistical significance. The golden (dark-golden) colored band represents the luminosity range (with a chosen lower limit of 1 fb^{-1}) for the LHC (proposed high luminosity LHC, HL-LHC).

extensions through different spin-zero multiplets that contain various electrically charged (singly, doubly, triply etc.) and often also neutral fields. In this paper we have entangled the CLFV and muon (g-2) data to constrain the relevant parameters associated with a doubly charged scalar through a simplified structure and also discuss the possible collider signatures. Further, focusing on the muon anomalous magnetic moment, we have assumed only a few non-zero Yukawa couplings, namely $y_{\mu\ell}$ with $\ell = e, \mu, \tau$, between the doubly charged scalar and the charged leptons. Furthermore, for simplicity we have chosen them real as well as $y_{\mu e} = y_{\mu\tau}$ and thus, left with only three relevant free parameters, namely $y_{\mu\mu}, y_{\mu e}(\equiv y_{\mu\tau})$ and $m_{\Delta^{\pm\pm}}$.

This simplified framework gives two additional contributions to the muon anomalous magnetic moment, as shown in Fig. 1. To start with we have computed contributions of these two new diagrams in $(g-2)_\mu$ as functions of the parameters $y_{\mu\mu}, y_{\mu e}(\equiv y_{\mu\tau})$ and $m_{\Delta^{\pm\pm}}$. Subsequently, we have scrutinized the impact of individual as well as combined contributions from $y_{\mu\mu}$ and $y_{\mu e}(\equiv y_{\mu\tau})$ on the $(g-2)_\mu$, for different choices of $m_{\Delta^{\pm\pm}}$. We have also explored various correlations among these three free parameters while analyzing Figs. 3–5. These correlations were used to extract the upper bounds on parameters $y_{\mu\mu}$ and $y_{\mu e}(\equiv y_{\mu\tau})$ as 1.2 and 0.3, respectively, keeping in mind their real nature and the span in $m_{\Delta^{\pm\pm}}$, i.e., 400 GeV—1000 GeV. In addition, these plots also provide the following observations: (1) Contribution from $y_{\mu e}(\equiv y_{\mu\tau})$ in the evaluation of Δa_μ is always negative. (2) The size of this contribution is negligible for $y_{\mu e}(\equiv y_{\mu\tau}) \lesssim 0.01$. In this region, the constraint on Δa_μ gets satisfied solely from $y_{\mu\mu}$ with $0.1 \lesssim y_{\mu\mu} \lesssim 0.3$. (3) In the span of $0.01 \lesssim y_{\mu e}(\equiv y_{\mu\tau}) \lesssim 0.1$, this contribution is comparable to the same coming from $y_{\mu\mu}$ (i.e., when $0.3 \lesssim y_{\mu\mu} \lesssim 0.6$) and, together they satisfy the constraint on Δa_μ through a *tuned* cancellation. (4) In the region $0.1 \lesssim y_{\mu e}(\equiv y_{\mu\tau}) \lesssim 0.3$, a large negative contribution from this parameter appears useful to compensate the large positive contribution from $y_{\mu\mu}$ with $y_{\mu\mu} \gtrsim 0.6$. In this corner of the parameter space, two large but opposite sign contributions partially cancel each other in a *much-tuned way* to satisfy the experimental bound on Δa_μ.

The chosen set of Yukawa couplings also generates new contributions to a class of CLFV processes, as addressed in Sec. IV. We have also investigated these processes in this paper in the light of parameters $y_{\mu\mu}, y_{\mu e}(\equiv y_{\mu\tau})$ and $m_{\Delta^{\pm\pm}}$, independent of the $(g-2)_\mu$ process. In the context of these analyses we observed that the allowed $y_{\mu\mu} - y_{\mu\ell}(\ell \neq \mu)$ parameter space prefers reciprocal behavior between the two aforementioned parameters. This feature is evident from Fig. 6. In these same set of plots we observed a significant enhancement of the surviving $y_{\mu\mu} - y_{\mu\ell}$ parameter space as one considers larger $m_{\Delta^{\pm\pm}}$ values. On the contrary, the allowed region in the $y_{\mu\mu} - y_{\mu\ell}$ parameter space shrinks when one considers more stringent expected future limits on different CLFV processes. As a final step of our analysis, we have explored the region of overlap among the different possible $y_{\mu\mu} - y_{\mu\ell}$ planes that can survive the *individual* constraints of various CLFV processes and $(g-2)_\mu$. Our investigation predicts a regime of overlap, i.e., $0.0001 \lesssim y_{\mu e}(\equiv y_{\mu\tau}) \lesssim 0.0004$, $0.1 \lesssim y_{\mu\mu} \lesssim 0.3$ for $m_{\Delta^{\pm\pm}} = 400$ GeV where all the *present* constraints on various CLFV processes and $(g-2)_\mu$ are simultaneously satisfied. This region, as can be seen from Fig. 6, expands slightly for $y_{\mu e}$, i.e., $0.0001 \lesssim y_{\mu e}(\equiv y_{\mu\tau}) \lesssim 0.0006$ while shifts for $y_{\mu\mu}$, i.e., $0.3 \lesssim y_{\mu\mu} \lesssim 0.6$ when one considers $m_{\Delta^{\pm\pm}} = 1000$ GeV. Expected improvements of the lower bounds for CLFV processes by a few orders of magnitude in the future, e.g., $R(\mu N \to eN^*)$ would washout any such common region where constraints on the CLFV processes and Δa_μ are simultaneously satisfied. Hence, any future measurements in this direction will discard the possibility that *only* a doubly charged scalar is instrumental for both the CLFV processes and the muon anomalous magnetic moment. In other words, given that one can achieve the proposed sensitivities for the CLFV processes in future and observe a region of overlap, the presence of certain other BSM particles is definitely guaranteed. One can nevertheless, revive some regime of overlap, even when only a doubly charged scalar is present, by considering a much larger $m_{\Delta^{\pm\pm}}$ which is experimentally less appealing.

Finally, we used our knowledge of $y_{\mu\mu}$, $y_{\mu e}(\equiv y_{\mu\tau})$ and $m_{\Delta^{\pm\pm}}$, that we have gathered while investigating a few CLFV processes and Δa_μ, in the context of a LHC study for $pp \to \Delta^{\pm\pm}\Delta^{\mp\mp} \to 2\ell_\alpha^\pm 2\ell_\beta^\mp$ processes. Our analysis of the Sec. V suggests that $y_{\mu\mu} \gg y_{\mu\ell}(\ell \neq \mu)$ when one simultaneously considers the existing set of constraints on the two concerned processes. Thus, in the context of the chosen simplified model framework, the decay mode $\Delta^{\pm\pm} \to \mu^\pm\mu^\pm$ dominates over the flavor violating $\Delta^{\pm\pm}$ decays. We have addressed the possibility of detecting our construction at the run-II of LHC with 13 TeV center-of-mass energy as a function of the integrated luminosity, for the three different sets of model parameters (see Fig. 7). One can conclude from the same plot that, provided the LHC will attain the proposed integrated luminosity of 300 fb^{-1}, a statistically significant (i.e., $\geq 4\sigma$) detection of the studied $\Delta^{\pm\pm}$ would remain well envisaged till $m_{\Delta^{\pm\pm}} \approx 800$ GeV. Probing higher $m_{\Delta^{\pm\pm}}$ values would require a high-luminosity collider. Lastly, we conclude that experimental status of the studied scenario with future generation CLFV measurements is rather critical, because: (1) One observes a region in the $y_{\mu\mu} - y_{\mu\ell}$ parameter space which satisfies both the constraints of muon $(g-2)$ and the set of leading CLFV processes for the range of 400 GeV $\lesssim m_{\Delta^{\pm\pm}} \lesssim$ 1000 GeV. Such an observation would signify the presence of some new particles, apart from a $\Delta^{\pm\pm}$. However, any

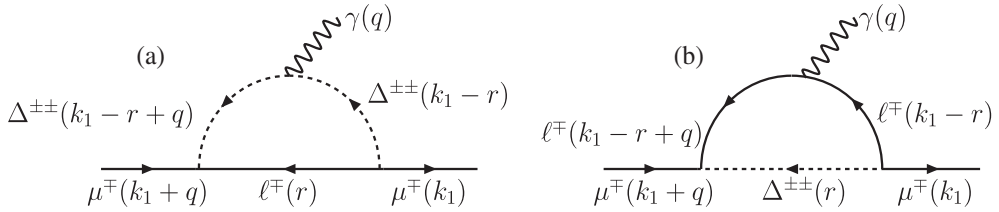

FIG. 8. Relevant details needed to compute Feynman amplitudes for the two diagrams shown in Fig. 1. The direction for all the momentum is from left to right and $k = k_1 + q$.

such additional information will increase the complexity of the underlying model at the cost of reduced predictability. (2) A similar region in the $y_{\mu\mu} - y_{\mu\ell}$ parameter space appears for a higher $m_{\Delta^{\pm\pm}}$ value, i.e., $m_{\Delta^{\pm\pm}} > 1000$ GeV. In this case, as can be seen from Fig. 7, the collider prospects of detecting such a heavy $m_{\Delta^{\pm\pm}}$ would appear rather poor, even at the proposed high luminosity LHC (HL-LHC) with an integrated luminosity of 3000 fb^{-1}.

ACKNOWLEDGMENTS

The work of J. C. is supported by the Department of Science & Technology, Government of INDIA under the Grant Agreement No. IFA12-PH-34 (INSPIRE Faculty Award). P. G. acknowledges the support from P2IO Excellence Laboratory (LABEX). The work of S. M. is partially supported by funding available from the Department of Atomic Energy, Government of India, for the Regional Centre for Accelerator-based Particle Physics (RECAPP), Harish-Chandra Research Institute.

APPENDIX:

In this appendix we present the calculation needed for the computation of $(g-2)_\mu$ through a $\Delta^{\pm\pm}$, as shown in Fig. 8. One may write down these two processes as $\mu(k_1+q) \to \mu(k_1) + \gamma(q)$, where k_1, q represent four-momentum of the incoming muon, the outgoing muon, and the outgoing photon, respectively.

The Feynman amplitude for the process leading to anomalous magnetic moment of muon can be written as:

$$i\mathcal{M}^\lambda = ie\left[\bar{u}(k_1+q)\left(\gamma^\lambda F_1(q^2) + i\frac{\sigma^{\lambda\nu}q_\nu}{2m_\mu}F_2(q^2)\right)u(k_1)\right], \tag{A1}$$

where $F_2|_{q^2=0}$ is the form factor which needs to be calculated.

The amplitude for the process shown in Fig. 8(a) is written as:

$$\begin{aligned} i\mathcal{M}_1^\dagger = &\int \frac{d^4r}{(2\pi)^4}\bar{u}(k_1+q)y_{\mu\ell}\frac{i(\not{r}+m_\ell)}{r^2-m_\ell^2}y_{\mu\ell} \\ &\times \frac{i}{(k_1-r+q)^2-m_{\Delta^{\pm\pm}}^2}\frac{i}{(k_1-r)^2-m_{\Delta^{\pm\pm}}^2} \\ &\times [-iQ_{\Delta^{\pm\pm}}[(k_1-r+q)+k_1-r]_\mu]u(k_1), \end{aligned} \tag{A2}$$

where $Q_{\Delta^{\pm\pm}} = 2e$ is the electric charge of the doubly charged scalar.

With the same spirit one can compute the contribution from the second diagram, as shown in Fig. 8(b), where the amplitude reads as:

$$\begin{aligned} i\mathcal{M}_2^\dagger = &\int \frac{d^4r}{(2\pi)^4}\bar{u}(k_1+q)y_{\mu\ell}\frac{i(\not{k}_1-\not{r}+m_\ell)}{(k_1-r)^2-m_\ell^2}(-ie\gamma^\mu) \\ &\times \frac{i(\not{k}_1-\not{r}+\not{q}+m_\ell)}{(k_1-r+q)^2-m_\ell^2}y_{\mu\ell}\frac{i}{(r^2-m_{\Delta^{\pm\pm}}^2)}u(k_1). \end{aligned} \tag{A3}$$

After combining these two contributions [Eqs. (A2), (A3)] and extracting the coefficient of $\sigma_{\mu\nu}$, after a few intermediate steps, we find the total contribution to muon $(g-2)$ as:

$$\begin{aligned} \Delta a_\mu = &\frac{f_m m_\mu^2 y_{\mu\ell}^2}{8\pi^2}\left[\int_0^1 d\rho \frac{2(\rho+\frac{m_\ell}{m_\mu})(\rho^2-\rho)}{[m_\mu^2\rho^2+(m_{\Delta^{\pm\pm}}^2-m_\mu^2)\rho+(1-\rho)m_\ell^2]}\right. \\ &\left. -\int_0^1 d\rho \frac{(\rho^2-\rho^3+\frac{m_\ell}{m_\mu}\rho^2)}{[m_\mu^2\rho^2+(m_\ell^2-m_\mu^2)\rho+(1-\rho)m_{\Delta^{\pm\pm}}^2]}\right]. \end{aligned} \tag{A4}$$

Here f_m is a multiplicative factor which is equal to 1 for $\ell = e, \tau$ while equals to 4 for $\ell = \mu$. The latter appears due to the presence of two identical fields in the interaction term.

[1] G. Aad *et al.* (ATLAS Collaboration), Phys. Lett. B **716**, 1 (2012).
[2] S. Chatrchyan *et al.* (CMS Collaboration), Phys. Lett. B **716**, 30 (2012).
[3] G. Aad *et al.* (ATLAS and CMS Collaborations), Phys. Rev. Lett. **114**, 191803 (2015).
[4] The ATLAS and CMS Collaborations, Report No. ATLAS-CONF-2015-044, 2015.
[5] K. A. Olive *et al.* (Particle Data Group), Chin. Phys. C **38**, 090001 (2014).
[6] H. Baer, T. Barklow, K. Fujii, Y. Gao, A. Hoang, S. Kanemura, J. List, H. E. Logan, A. Nomerotski, M. Perelstein *et al.*, arXiv:1306.6352.
[7] D. V. Forero, M. Tortola, and J. W. F. Valle, Phys. Rev. D **86**, 073012 (2012).
[8] G. L. Fogli, E. Lisi, A. Marrone, D. Montanino, A. Palazzo, and A. M. Rotunno, Phys. Rev. D **86**, 013012 (2012).
[9] M. C. Gonzalez-Garcia, M. Maltoni, J. Salvado, and T. Schwetz, J. High Energy Phys. 12 (2012) 123.
[10] M. Sher, Phys. Rep. **179**, 273 (1989).
[11] J. Elias-Miro, J. R. Espinosa, G. F. Giudice, H. M. Lee, and A. Strumia, J. High Energy Phys. 06 (2012) 031.
[12] S. Alekhin, A. Djouadi, and S. Moch, Phys. Lett. B **716**, 214 (2012).
[13] D. Buttazzo, G. Degrassi, P. P. Giardino, G. F. Giudice, F. Sala, A. Salvio, and A. Strumia, J. High Energy Phys. 12 (2013) 089.
[14] F. Jegerlehner, Acta Phys. Pol. B **45**, 1167 (2014).
[15] A. Djouadi, Phys. Rep. **457**, 1 (2008).
[16] A. Djouadi, Phys. Rep. **459**, 1 (2008).
[17] J. C. Pati and A. Salam, Phys. Rev. D **10**, 275 (1974); **11**, 703(E) (1975).
[18] R. N. Mohapatra and J. C. Pati, Phys. Rev. D **11**, 566 (1975).
[19] R. N. Mohapatra and J. C. Pati, Phys. Rev. D **11**, 2558 (1975).
[20] G. Senjanovic and R. N. Mohapatra, Phys. Rev. D **12**, 1502 (1975).
[21] W. Konetschny and W. Kummer, Phys. Lett. B **70**, 433 (1977).
[22] G. Senjanovic, Nucl. Phys. **B153**, 334 (1979).
[23] M. Magg and C. Wetterich, Phys. Lett. B **94**, 61 (1980).
[24] J. Schechter and J. W. F. Valle, Phys. Rev. D **22**, 2227 (1980).
[25] T. P. Cheng and L.-F. Li, Phys. Rev. D **22**, 2860 (1980).
[26] A. Zee, Phys. Lett. B **93**, 389 (1980); **95**, 461 (1980).
[27] G. Lazarides, Q. Shafi, and C. Wetterich, Nucl. Phys. **B181**, 287 (1981).
[28] R. N. Mohapatra and G. Senjanovic, Phys. Rev. D **23**, 165 (1981).
[29] A. Zee, Phys. Lett. B **161**, 141 (1985).
[30] H. Georgi and M. Machacek, Nucl. Phys. **B262**, 463 (1985).
[31] M. S. Chanowitz and M. Golden, Phys. Lett. B **165**, 105 (1985).
[32] A. Zee, Nucl. Phys. **B264**, 99 (1986).
[33] K. S. Babu, Phys. Lett. B **203**, 132 (1988).
[34] J. McDonald, Phys. Rev. D **50**, 3637 (1994).
[35] M. C. Bento, O. Bertolami, R. Rosenfeld, and L. Teodoro, Phys. Rev. D **62**, 041302 (2000).
[36] C. P. Burgess, M. Pospelov, and T. ter Veldhuis, Nucl. Phys. **B619**, 709 (2001).
[37] K. S. Babu and C. Macesanu, Phys. Rev. D **67**, 073010 (2003).
[38] H. Davoudiasl, R. Kitano, T. Li, and H. Murayama, Phys. Lett. B **609**, 117 (2005).
[39] R. Schabinger and J. D. Wells, Phys. Rev. D **72**, 093007 (2005).
[40] M. Cirelli, N. Fornengo, and A. Strumia, Nucl. Phys. **B753**, 178 (2006).
[41] A. Kusenko, Phys. Rev. Lett. **97**, 241301 (2006).
[42] C.-S. Chen, C. Q. Geng, and J. N. Ng, Phys. Rev. D **75**, 053004 (2007).
[43] D. O'Connell, M. J. Ramsey-Musolf, and M. B. Wise, Phys. Rev. D **75**, 037701 (2007).
[44] O. Bahat-Treidel, Y. Grossman, and Y. Rozen, J. High Energy Phys. 05 (2007) 022.
[45] C.-S. Chen, C.-Q. Geng, J. N. Ng, and J. M. S. Wu, J. High Energy Phys. 08 (2007) 022.
[46] I. Gogoladze, N. Okada, and Q. Shafi, Phys. Rev. D **78**, 085005 (2008).
[47] V. Barger, P. Langacker, M. McCaskey, M. Ramsey-Musolf, and G. Shaughnessy, Phys. Rev. D **79**, 015018 (2009).
[48] T. Hambye, F. S. Ling, L. Lopez Honorez, and J. Rocher, J. High Energy Phys. 07 (2009) 090; 05 (2010) 066.
[49] S. Dawson and W. Yan, Phys. Rev. D **79**, 095002 (2009).
[50] K. S. Babu, S. Nandi, and Z. Tavartkiladze, Phys. Rev. D **80**, 071702 (2009).
[51] M. Gonderinger, Y. Li, H. Patel, and M. J. Ramsey-Musolf, J. High Energy Phys. 01 (2010) 053.
[52] M. Aoki, S. Kanemura, and K. Yagyu, Phys. Lett. B **702**, 355 (2011); **706**, 495(E) (2012).
[53] F. del Aguila, A. Aparici, S. Bhattacharya, A. Santamaria, and J. Wudka, J. High Energy Phys. 05 (2012) 133.
[54] O. Lebedev, Eur. Phys. J. C **72**, 2058 (2012).
[55] E. J. Chun, H. M. Lee, and P. Sharma, J. High Energy Phys. 11 (2012) 106.
[56] W. Chao, M. Gonderinger, and M. J. Ramsey-Musolf, Phys. Rev. D **86**, 113017 (2012).
[57] P. Bhupal Dev, D. K. Ghosh, N. Okada, and I. Saha, J. High Energy Phys. 03 (2013) 150; 05 (2013) 049.
[58] J. Barry and W. Rodejohann, J. High Energy Phys. 09 (2013) 153.
[59] J. M. Cline, K. Kainulainen, P. Scott, and C. Weniger, Phys. Rev. D **88**, 055025 (2013); **92**, 039906(E) (2015).
[60] J. Chakrabortty, P. Konar, and T. Mondal, Phys. Rev. D **89**, 056014 (2014).
[61] J. Chakrabortty, P. Konar, and T. Mondal, Phys. Rev. D **89**, 095008 (2014).
[62] S. F. King, A. Merle, and L. Panizzi, J. High Energy Phys. 11 (2014) 124.
[63] H. Okada, T. Toma, and K. Yagyu, Phys. Rev. D **90**, 095005 (2014).
[64] R. Costa, A. P. Morais, M. O. P. Sampaio, and R. Santos, Phys. Rev. D **92**, 025024 (2015).
[65] V. Martín Lozano, J. M. Moreno, and C. B. Park, J. High Energy Phys. 08 (2015) 004.
[66] A. Falkowski, C. Gross, and O. Lebedev, J. High Energy Phys. 05 (2015) 057.
[67] C. Bonilla, R. M. Fonseca, and J. W. F. Valle, Phys. Lett. B **756**, 345 (2016).

[68] H. Okada and K. Yagyu, Phys. Rev. D **93**, 013004 (2016).
[69] A. Das, N. Okada, and N. Papapietro, arXiv:1509.01466.
[70] G. Bambhaniya, P. S. B. Dev, S. Goswami, and M. Mitra, J. High Energy Phys. 04 (2016) 046.
[71] T. Blank and W. Hollik, Nucl. Phys. **B514**, 113 (1998).
[72] A. Melfo, M. Nemevsek, F. Nesti, G. Senjanovic, and Y. Zhang, Phys. Rev. D **85**, 055018 (2012).
[73] C. Bonilla, R. M. Fonseca, and J. W. F. Valle, Phys. Rev. D **92**, 075028 (2015).
[74] J. F. Gunion, C. Loomis, and K. T. Pitts, in *1996 DPF / DPB Summer Study On New Directions For High-Energy Physics: Proceedings, Snowmass 1996*, eConf C960625, LTH096 (1996), arXiv:hep-ph/9610237.
[75] S. Chakrabarti, D. Choudhury, R. M. Godbole, and B. Mukhopadhyaya, Phys. Lett. B **434**, 347 (1998).
[76] E. J. Chun, K. Y. Lee, and S. C. Park, Phys. Lett. B **566**, 142 (2003).
[77] M. Muhlleitner and M. Spira, Phys. Rev. D **68**, 117701 (2003).
[78] A. G. Akeroyd and M. Aoki, Phys. Rev. D **72**, 035011 (2005).
[79] T. Han, B. Mukhopadhyaya, Z. Si, and K. Wang, Phys. Rev. D **76**, 075013 (2007).
[80] J. Garayoa and T. Schwetz, J. High Energy Phys. 03 (2008) 009.
[81] M. Kadastik, M. Raidal, and L. Rebane, Phys. Rev. D **77**, 115023 (2008).
[82] A. G. Akeroyd, M. Aoki, and H. Sugiyama, Phys. Rev. D **77**, 075010 (2008).
[83] P. Fileviez Perez, T. Han, G.-y. Huang, T. Li, and K. Wang, Phys. Rev. D **78**, 015018 (2008).
[84] F. del Aguila and J. A. Aguilar-Saavedra, Nucl. Phys. **B813**, 22 (2009).
[85] A. G. Akeroyd and C.-W. Chiang, Phys. Rev. D **80**, 113010 (2009).
[86] A. Maiezza, M. Nemevsek, F. Nesti, and G. Senjanovic, Phys. Rev. D **82**, 055022 (2010).
[87] A. G. Akeroyd, C.-W. Chiang, and N. Gaur, J. High Energy Phys. 11 (2010) 005.
[88] V. Tello, M. Nemevsek, F. Nesti, G. Senjanovic, and F. Vissani, Phys. Rev. Lett. **106**, 151801 (2011).
[89] V. Rentala, W. Shepherd, and S. Su, Phys. Rev. D **84**, 035004 (2011).
[90] A. G. Akeroyd and H. Sugiyama, Phys. Rev. D **84**, 035010 (2011).
[91] M. Aoki, S. Kanemura, and K. Yagyu, Phys. Rev. D **85**, 055007 (2012).
[92] A. G. Akeroyd, S. Moretti, and H. Sugiyama, Phys. Rev. D **85**, 055026 (2012).
[93] J. Chakrabortty, J. Gluza, R. Sevillano, and R. Szafron, J. High Energy Phys. 07 (2012) 038.
[94] S. P. Das, F. F. Deppisch, O. Kittel, and J. W. F. Valle, Phys. Rev. D **86**, 055006 (2012).
[95] E. J. Chun and P. Sharma, J. High Energy Phys. 08 (2012) 162.
[96] C.-S. Chen, C.-Q. Geng, D. Huang, and L.-H. Tsai, Phys. Rev. D **87**, 077702 (2013).
[97] S. Kanemura, K. Yagyu, and H. Yokoya, Phys. Lett. B **726**, 316 (2013).
[98] G. Bambhaniya, J. Chakrabortty, S. Goswami, and P. Konar, Phys. Rev. D **88**, 075006 (2013).
[99] F. del Aguila, M. Chala, A. Santamaria, and J. Wudka, Phys. Lett. B **725**, 310 (2013).
[100] E. J. Chun and P. Sharma, Phys. Lett. B **728**, 256 (2014).
[101] F. del guila and M. Chala, J. High Energy Phys. 03 (2014) 027.
[102] G. Bambhaniya, J. Chakrabortty, J. Gluza, M. Kordiaczyńska, and R. Szafron, J. High Energy Phys. 05 (2014) 033.
[103] B. Dutta, R. Eusebi, Y. Gao, T. Ghosh, and T. Kamon, Phys. Rev. D **90**, 055015 (2014).
[104] S. Kanemura, K. Tsumura, K. Yagyu, and H. Yokoya, Phys. Rev. D **90**, 075001 (2014).
[105] S. Kanemura, M. Kikuchi, K. Yagyu, and H. Yokoya, Phys. Rev. D **90**, 115018 (2014).
[106] G. Bambhaniya, J. Chakrabortty, J. Gluza, T. Jeliński, and M. Kordiaczyńska, Phys. Rev. D **90**, 095003 (2014).
[107] F. F. Deppisch, T. E. Gonzalo, S. Patra, N. Sahu, and U. Sarkar, Phys. Rev. D **91**, 015018 (2015).
[108] Z.-L. Han, R. Ding, and Y. Liao, Phys. Rev. D **91**, 093006 (2015).
[109] G. Bambhaniya, J. Chakrabortty, J. Gluza, T. Jeliński, and R. Szafron, Phys. Rev. D **92**, 015016 (2015).
[110] P. D. Acton *et al.* (OPAL Collaboration), Phys. Lett. B **295**, 347 (1992).
[111] G. Abbiendi *et al.* (OPAL Collaboration), Phys. Lett. B **526**, 221 (2002).
[112] J. Abdallah *et al.* (DELPHI Collaboration), Phys. Lett. B **552**, 127 (2003).
[113] G. Abbiendi *et al.* (OPAL Collaboration), Phys. Lett. B **577**, 93 (2003).
[114] P. Achard *et al.* (L3 Collaboration), Phys. Lett. B **576**, 18 (2003).
[115] V. M. Abazov *et al.* (D0 Collaboration), Phys. Rev. Lett. **93**, 141801 (2004).
[116] D. Acosta *et al.* (CDF Collaboration), Phys. Rev. Lett. **93**, 221802 (2004).
[117] G. Azuelos, K. Benslama, and J. Ferland, J. Phys. G **32**, 73 (2006).
[118] T. Rommerskirchen and T. Hebbeker, J. Phys. G **34**, N47 (2007).
[119] A. Hektor, M. Kadastik, M. Muntel, M. Raidal, and L. Rebane, Nucl. Phys. **B787**, 198 (2007).
[120] V. M. Abazov *et al.* (D0 Collaboration), Phys. Rev. Lett. **101**, 071803 (2008).
[121] T. Aaltonen *et al.* (CDF Collaboration), Phys. Rev. Lett. **101**, 121801 (2008).
[122] V. M. Abazov *et al.* (D0 Collaboration), Phys. Rev. Lett. **108**, 021801 (2012).
[123] T. Aaltonen *et al.* (CDF Collaboration), Phys. Rev. Lett. **107**, 181801 (2011).
[124] S. Chatrchyan *et al.* (CMS Collaboration), Eur. Phys. J. C **72**, 2189 (2012).
[125] G. Aad *et al.* (ATLAS Collaboration), Eur. Phys. J. C **72**, 2244 (2012).
[126] G. Aad *et al.* (ATLAS Collaboration), J. High Energy Phys. 03 (2015) 041.
[127] S. T. Petcov, Phys. Lett. B **115**, 401 (1982).
[128] G. K. Leontaris, K. Tamvakis, and J. D. Vergados, Phys. Lett. B **162**, 153 (1985).
[129] J. Bernabeu, A. Pich, and A. Santamaria, Z. Phys. C **30**, 213 (1986).

[130] S. M. Bilenky and S. T. Petcov, Rev. Mod. Phys. **59**, 671 (1987); **60**, 575(E) (1988); **61**, 169(E) (1989).
[131] M. L. Swartz, Phys. Rev. D **40**, 1521 (1989).
[132] M. Kakizaki, Y. Ogura, and F. Shima, Phys. Lett. B **566**, 210 (2003).
[133] V. Cirigliano, A. Kurylov, M. J. Ramsey-Musolf, and P. Vogel, Phys. Rev. D **70**, 075007 (2004).
[134] V. Cirigliano, A. Kurylov, M. J. Ramsey-Musolf, and P. Vogel, Phys. Rev. Lett. **93**, 231802 (2004).
[135] A. Abada, C. Biggio, F. Bonnet, M. B. Gavela, and T. Hambye, J. High Energy Phys. 12 (2007) 061.
[136] T. Fukuyama, H. Sugiyama, and K. Tsumura, J. High Energy Phys. 03 (2010) 044.
[137] B. Ren, K. Tsumura, and X.-G. He, Phys. Rev. D **84**, 073004 (2011).
[138] J. Chakrabortty, P. Ghosh, and W. Rodejohann, Phys. Rev. D **86**, 075020 (2012).
[139] D. N. Dinh, A. Ibarra, E. Molinaro, and S. T. Petcov, J. High Energy Phys. 08 (2012) 125; 09 (2013) 023.
[140] B. P. Nayak and M. K. Parida, Eur. Phys. J. C **75**, 183 (2015).
[141] M. Borah, D. Borah, M. K. Das, and S. Patra, Phys. Rev. D **90**, 095020 (2014).
[142] R. N. Mohapatra and J. D. Vergados, Phys. Rev. Lett. **47**, 1713 (1981).
[143] W. C. Haxton, S. P. Rosen, and G. J. Stephenson, Phys. Rev. D **26**, 1805 (1982).
[144] L. Wolfenstein, Phys. Rev. D **26**, 2507 (1982).
[145] M. Hirsch, H. V. Klapdor-Kleingrothaus, and O. Panella, Phys. Lett. B **374**, 7 (1996).
[146] J. Chakrabortty, H. Z. Devi, S. Goswami, and S. Patra, J. High Energy Phys. 08 (2012) 008.
[147] P. Bhupal Dev, S. Goswami, and M. Mitra, Phys. Rev. D **91**, 113004 (2015).
[148] C. Picciotto, Phys. Rev. D **56**, 1612 (1997).
[149] Y.-L. Ma, Phys. Rev. D **79**, 033014 (2009).
[150] N. Quintero, Phys. Rev. D **87**, 056005 (2013).
[151] G. Bambhaniya, J. Chakrabortty, and S. K. Dagaonkar, Phys. Rev. D **91**, 055020 (2015).
[152] A. Freitas, J. Lykken, S. Kell, and S. Westhoff, J. High Energy Phys. 05 (2014) 145; 09 (2014) 155(E).
[153] A. Atre, T. Han, S. Pascoli, and B. Zhang, J. High Energy Phys. 05 (2009) 030.
[154] M. Kohda, H. Sugiyama, and K. Tsumura, Phys. Lett. B **718**, 1436 (2013).
[155] M. Gustafsson, J. M. No, and M. A. Rivera, Phys. Rev. Lett. **110**, 211802 (2013); **112**, 259902(E) (2014).
[156] K. Yagyu, arXiv:1304.6338.
[157] I. Picek and B. Radovcic, Phys. Lett. B **687**, 338 (2010).
[158] K. Kumericki, I. Picek, and B. Radovcic, Phys. Rev. D **84**, 093002 (2011).
[159] K. Earl, K. Hartling, H. E. Logan, and T. Pilkington, Phys. Rev. D **90**, 055029 (2014); **92**, 039902(E) (2015).
[160] K. Hally, H. E. Logan, and T. Pilkington, Phys. Rev. D **85**, 095017 (2012).
[161] J. Hisano and K. Tsumura, Phys. Rev. D **87**, 053004 (2013).
[162] S. Kanemura, M. Kikuchi, and K. Yagyu, Phys. Rev. D **88**, 015020 (2013).
[163] K. Earl, K. Hartling, H. E. Logan, and T. Pilkington, Phys. Rev. D **88**, 015002 (2013).
[164] A. Nyffeler, Nuovo Cim. Soc. Ital. Fis. **C037**, 173 (2014); Int. J. Mod. Phys. Conf. Ser. **35**, 1460456 (2014).
[165] J. Adam *et al.* (MEG Collaboration), Phys. Rev. Lett. **110**, 201801 (2013).
[166] P. A. R. Ade *et al.* (Planck Collaboration), arXiv: 1502.01589.
[167] G. W. Bennett *et al.* (Muon g-2 Collaboration), Phys. Rev. D **73**, 072003 (2006).
[168] B. L. Roberts, Chin. Phys. C **34**, 741 (2010).
[169] J. Prades, E. de Rafael, and A. Vainshtein, Adv. Ser. Dir. High Energy Phys. **20**, 303 (2009).
[170] A. Nyffeler, Chin. Phys. C **34**, 705 (2010).
[171] M. Davier, A. Hoecker, B. Malaescu, and Z. Zhang, Eur. Phys. J. C **71**, 1515 (2011); **72**, 1874(E) (2012).
[172] K. Hagiwara, R. Liao, A. D. Martin, D. Nomura, and T. Teubner, J. Phys. G **38**, 085003 (2011).
[173] M. Knecht, Int. J. Mod. Phys. Conf. Ser. **35**, 1460405 (2014).
[174] J. P. Leveille, Nucl. Phys. **B137**, 63 (1978).
[175] S. R. Moore, K. Whisnant, and B.-L. Young, Phys. Rev. D **31**, 105 (1985).
[176] M. Hirsch, F. Staub, and A. Vicente, Phys. Rev. D **85**, 113013 (2012); **91**, 059902(E) (2015).
[177] F. Wilczek and A. Zee, Phys. Rev. Lett. **38**, 531 (1977).
[178] S. B. Treiman, F. Wilczek, and A. Zee, Phys. Rev. D **16**, 152 (1977).
[179] G. Altarelli, L. Baulieu, N. Cabibbo, L. Maiani, and R. Petronzio, Nucl. Phys. **B125**, 285 (1977); **B130**, 516 (1977).
[180] W. J. Marciano and A. I. Sanda, Phys. Rev. Lett. **38**, 1512 (1977).
[181] M. Raidal and A. Santamaria, Phys. Lett. B **421**, 250 (1998).
[182] A. G. Akeroyd, M. Aoki, and H. Sugiyama, Phys. Rev. D **79**, 113010 (2009).
[183] R. Kitano, M. Koike, and Y. Okada, Phys. Rev. D **66**, 096002 (2002); **76**, 059902(E) (2007).
[184] A. M. Baldini *et al.*, arXiv:1301.7225.
[185] B. Aubert *et al.* (*BABAR* Collaboration), Phys. Rev. Lett. **104**, 021802 (2010).
[186] T. Aushev *et al.*, arXiv:1002.5012.
[187] K. Hayasaka *et al.*, Phys. Lett. B **687**, 139 (2010).
[188] W. H. Bertl *et al.* (SINDRUM II Collaboration), Eur. Phys. J. C **47**, 337 (2006).
[189] L. Bartoszek *et al.* (Mu2e Collaboration), arXiv: 1501.05241.
[190] A. Belyaev, N. D. Christensen, and A. Pukhov, Comput. Phys. Commun. **184**, 1729 (2013).
[191] T. Sjostrand, S. Mrenna, and P. Z. Skands, J. High Energy Phys. 05 (2006) 026.
[192] J. Pumplin, D. R. Stump, J. Huston, H. L. Lai, P. M. Nadolsky, and W. K. Tung, J. High Energy Phys. 07 (2002) 012.
[193] J. Alwall, M. Herquet, F. Maltoni, O. Mattelaer, and T. Stelzer, J. High Energy Phys. 06 (2011) 128.
[194] J. Alwall, R. Frederix, S. Frixione, V. Hirschi, F. Maltoni, O. Mattelaer, H.-S. Shao, T. Stelzer, P. Torrielli, and M. Zaro, J. High Energy Phys. 07 (2014) 079.
[195] High Luminosity Large Hadron Collider, http://hilumilhc.web.cern.ch/.